

**Galaxy-Galaxy Weak Gravitational Lensing in Cluster
Environments**

by

Timothy James



A thesis Submitted to
The University of Birmingham
For the degree of
Master of Philosophy

UNIVERSITY OF
BIRMINGHAM

University of Birmingham Research Archive

e-theses repository

This unpublished thesis/dissertation is copyright of the author and/or third parties. The intellectual property rights of the author or third parties in respect of this work are as defined by The Copyright Designs and Patents Act 1988 or as modified by any successor legislation.

Any use made of information contained in this thesis/dissertation must be in accordance with that legislation and must be properly acknowledged. Further distribution or reproduction in any format is prohibited without the permission of the copyright holder.

Abstract

An investigation was carried out into the phenomenon of galaxy-galaxy weak lensing in a sample of 10 X-ray selected galaxy clusters. Using high resolution Hubble Space Telescope imaging data and mathematical techniques described within, the feasibility of detecting a galaxy-galaxy shear signal was demonstrated. A study was then carried out to assess the magnitude of the systematic effect of improper cluster-scale shear signal subtraction that had previously not been explicitly tested. It was found that the systematic effect was negligible compared to the shear signal of interest in all but one fairly extreme case. This is of interest to future studies in this field as it avoids the need for time-expensive detailed cluster models to be made before the relevant data can be extracted. The investigation also details the process of designing telescope masks for two world-leading spectroscopic instruments. Such observations are key in obtaining redshift constraints on strongly lensed arcs allowing normalisation of the cluster mass distribution and therefore determination of cluster masses.

Synopsis

The study of the constituent components of the universe at large has been one of the primary focuses in the human pursuit of knowledge. With the accelerating pace of change in the modern scientific world bringing ever newer technologies and revolutions in thinking, we are now on the verge of being able to directly measure contributions to the makeup of the universe.

The investigation of dark matter is a key part of understanding both the nature and assembly history of the universe. The nature of this dark matter however, prohibits us (at the time of writing) from detecting it directly. Instead, we are currently limited to measuring its effects on luminous, Baryonic matter after having made assumptions on the composition of the dark matter itself. Of all the methods currently available to detect and quantify dark matter, it is perhaps Gravitational Lensing that shows the most promise as it allows detailed information to be inferred about the mass and structure of dark matter in a wide variety of astronomical environments.

Acknowledgements

I thank my supervisor, Dr. Graham Smith for all his support and guidance in this investigation. Also Dr. Chris Haines, Dr. Johan Richard, Mr. Paul May and Miss Victoria Hamilton Morris for some excellent discussions on the topics considered in this study. I express huge gratitude to Miss Chiara Mingarelli, Miss Lyn Rycroft and Mr. Phil Brown for buoying me up during difficult days on the project and for being generally wonderful sources of support throughout my time at Birmingham. Special mention to Mr Adam Whittingham, Miss Anna Kennedy, Mr. Rob Sleath and Mr. Aaron Tighe for all their encouragement and occasionally giving me some temporary escape when things didn't go so well! Last but not least I thank my parents for their unceasing support through the good and bad times, I wouldn't have persevered without them.

Contents

1	Introduction	1
1.1	Lensing Theory	2
1.1.1	Deflection of Light	3
1.1.2	The Lens Equation	3
1.1.3	Image Distortion	4
1.2	Weak Lensing	5
1.3	Previous Work in this Field	6
1.3.1	The Development of Galaxy-Galaxy Weak Lensing	6
1.3.2	Studies of Galaxy-Galaxy Weak Lensing in Cluster Cores	7
1.3.3	Galaxy-galaxy Weak Lensing Beyond Cluster Cores	10
1.4	New Observations	11
1.4.1	This Thesis	12
2	Galaxy-Galaxy Weak Lensing	13
2.1	Data and Analysis	13
2.2	Results and Discussion	17
3	Galaxy-Galaxy Weak Lensing Simulations	23
3.1	Simulation Design	23
3.2	Preliminary Simulation Results	25
3.3	Simulation Refinement	30
4	Mask Design	38
4.1	Cluster Observations	38
4.2	Mask Design	38
4.3	VLT FORS2	40
5	Conclusions	44
6	Appendix: Cluster Strong-Lensing Observation Images	46

Chapter 1

Introduction

The standard cosmological model or Λ CDM model of the universe describes large scale dynamics and structure formation and is well supported by observations, most notably the WMAP mission [9]. It attributes a large proportion (73%) of the energy density of the universe at the current epoch to dark energy, which may be represented by the cosmological constant, Λ . Of the remaining 27% of the energy density, around 85% is believed to consist of cold dark matter with the remainder being the more familiar visible baryonic matter. The evolution of structure in the universe stems from primordial fluctuations in the cosmic microwave background (CMB). High sigma fluctuations in the spatial power spectrum of the CMB evolved into the first structures by gravitational collapse. These dark matter dominated concentrations formed aggregations along filaments and acted as a focus for further gravitational collapse. These dark matter 'halos' are the foundation of gravitationally bound systems containing both dark and baryonic matter that we now identify as galaxies, groups and clusters. By gravitational interaction, dark matter halos accrete mass via mergers along the large scale filamentary structure of the universe, contributing to the formation of progressively larger structures.

Clusters of galaxies are the largest and most recently formed large scale structures in the known universe. They are the pinnacle of the bottom-up hierarchy of large scale structure formation that has, up to the present epoch, been observed. The bottom-up hierarchy of structure formation dictates that the smallest components of cosmic structure, ie. the galaxies formed at the earliest epoch of the universe and that these 'building blocks' of structure have, since then, assembled into galaxy groups and eventually galaxy clusters via mergers driven by the gravitational attraction of their dark matter halos.

Galaxy clusters are therefore an excellent environment in which to examine the properties of galaxy-scale dark matter halos and how they evolve during the process of infall into the cluster as well as examination of the cluster-scale dark matter halo which comprises the vast majority of the structure's mass.

The issue with studying dark matter halos is the nature of dark matter itself. Dark matter has not been observed to emit radiation and therefore is effectively invisible to instruments across the whole of the electromagnetic spectrum. Direct observation of dark matter is, therefore, currently impossible and it is the gravitational effects that dark matter has on visible, baryonic matter that must be relied on for its study. Since the only way dark matter interacts, either with baryonic matter or itself, is via gravitational interaction, the phenomena used for its study must be based on gravitation. Due to the high masses of the objects under consideration in the study of galaxy clusters (masses of individual galaxies are of the order $10^{12} M_{\odot}$ while the clusters themselves total around $10^{15} M_{\odot}$), gravitational

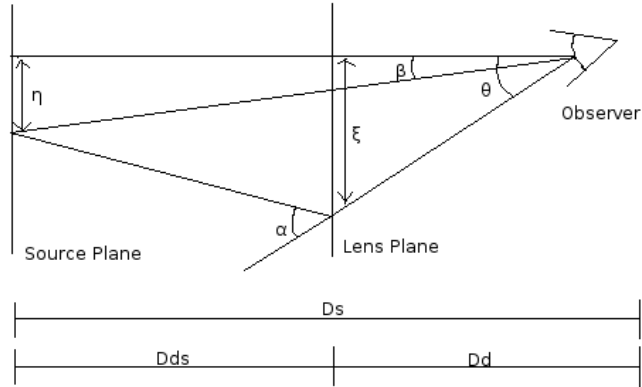


Figure 1.1: A simple ray diagram showing relevant angles for the deflection of a light ray by a simple mass distribution.

lensing becomes a powerful tool for measuring the density profiles of collapsed dark matter halos that host galaxies, groups and clusters.

1.1 Lensing Theory

Gravitational lensing as currently understood, was originally predicted by Einstein's General Theory of Relativity due to the property of mass that it distorts the space-time around it leading to light rays apparently being curved when they pass near to a massive object. The effect on most scales is tiny and undetectable. Fritz Zwicky first proposed that this property would lead to gravitational lenses being formed by the most massive virialised structures in the universe, namely galaxy clusters [33]. These objects gave viable opportunities for observing gravitational lensing in action, their great mass allowing the effect to be clearly observable (although the observations at the time were resolution and depth limited, the proposed deflection angles were considered feasible to observe). The first observation of any form of gravitational lensing was by Arthur Eddington during a 1919 solar eclipse [5]. This observation noted that stars appeared out of their known positions indicating that their light had been perturbed by the gravitational field of the sun. Multiple imaging due to gravitational lensing was first observed in the quasar system Q0957+561 in 1979. [31] A later development of particular interest for the work in this report was the first instance of the detection of gravitationally lensed arcs in a galaxy cluster environment by Soucail et al. (1986) which was initially thought to be an anomalously blue ring structure at the same redshift as the cluster Abell 370 ($z=0.374$) [26]. This object was later spectroscopically confirmed to lie at a significantly higher redshift than the cluster ($z=0.724$) with its arc shape due to lensing distortion [27].

The following is a brief introduction to lensing theory which is relevant to the methods described later in this report. For a more rigorous treatment of gravitational lensing, the reader is referred to the introduction to gravitational lensing by P. Schneider 2005 [24]

1.1.1 Deflection of Light

The simplest case of gravitational deflection of light is that of a point mass lens. Consider a ray bundle that passes close to an object but outside the Schwarzschild radius of the object. The impact parameter ξ is the distance of approach of the ray bundle passing the lensing mass, M . From General Relativity, the angle of deflection due to the light ray passing the mass is given by:

$$\alpha = \frac{4GM}{c^2\xi} \quad (1.1)$$

By adhering to the assumption that the gravitational field strength must be small an important simplifying assumption may be made in which the deflection due to an extended mass distribution may be expressed simply as the vector sum of its individual mass components. This allows a complex distribution of mass to be dealt with piecewise as a sum of mass elements, dm . A light ray passing a mass distribution on this scale will be deflected but the interval of space over which the deflection occurs compared to the distances between the ray source, the mass distribution and a distant observer, is so small (perhaps a megaparsec to traverse the cluster in a total path length of several gigaparsecs) that the ray path may be approximated to a straight line with a sudden deflection in the vicinity of the mass distribution. This allows the thin-lens approximation to be used which greatly simplifies the geometry of the lensing problem.

Defining the surface mass density of the lensing mass by

$$\Sigma(\xi) = \int dr'_3 \rho(\xi'_1, \xi'_2, r'_3) \quad (1.2)$$

(where (ξ'_1, ξ'_2, r'_3) are the spatial coordinates of a mass element dm) and the deflection angle (totalled over all mass elements) as

$$\alpha(\xi) = \frac{4G}{c^2} \int d^2\xi' \int dr'_3 \rho(\xi'_1, \xi'_2, r'_3) \frac{\xi - \xi'}{|\xi - \xi'|^2} \quad (1.3)$$

Substitution gives the final expression for the deflection angle given the surface mass density

$$\alpha(\xi) = \frac{4G}{c^2} \int d^2\xi' \Sigma(\xi') \frac{\xi - \xi'}{|\xi - \xi'|^2} \quad (1.4)$$

1.1.2 The Lens Equation

To interpret gravitational lensing observations, one needs to relate observed position and properties of lensed galaxies to their intrinsic properties and also to the mass distribution of the lens. In order to find the true position of the source, given the apparent position on the sky (or vice-versa), the Lens Equation is needed. A useful feature of the study of lensing on astrophysical scales is that the angles involved are extremely small and so the small-angle approximation where $\sin\alpha \approx \alpha$ may be used in what follows.

From Fig. 1.1, η is the vector of the source in the source plane and may be expressed as

$$\eta = \frac{D_s}{D_d} \xi - D_{ds} \alpha(\xi) \quad (1.5)$$

which through use of the angular identities $\eta = D_s\beta$ and $\xi = D_d\theta$ may be expressed as

$$\beta = \theta - \frac{D_{ds}}{D_s}\alpha(D_d\theta) = \theta - \alpha(\theta) \quad (1.6)$$

This gives rise to the possibility that more than one solution may exist for the image position, θ given a true source position, β . The physical interpretation of this is that under the condition that the surface mass density of the lens exceeds a critical value, the source will be multiply imaged on the sky, leading to observations of multiple images of the same background source. Under these conditions, the lensing is said to be in the Strong regime. For strong lensing to occur, the mean projected density interior to the lensing radius under consideration must exceed the critical density, ie. $\langle\kappa\rangle$ must be equal to or greater than 1. The convergence is given by

$$\kappa(\theta) = \frac{\Sigma(D_d\theta)}{\Sigma_{cr}} \quad (1.7)$$

The critical density required for strong lensing to take place is expressed as

$$\Sigma_{cr} = \frac{c^2}{4\pi G} \frac{D_s}{D_d D_{ds}} \quad (1.8)$$

and is a function of the geometry of the lens system dependent on D_{ds} , D_s and D_d .

The deflection angle may also be written in terms of the potential of the mass distribution of the lens

$$\psi(\theta) = \frac{1}{\pi} \int d^2\theta' \kappa(\theta') \ln|\theta - \theta'| \quad (1.9)$$

where

$$\alpha = \nabla\psi \quad (1.10)$$

1.1.3 Image Distortion

The images of background sources that lensing produces differ strongly based on their position relative to the mass distribution of the lens. Since during the process of light deflection by a massive object, no extra photons from the source are added or removed, the brightness distribution of the object in the lens plane may be expressed as

$$I(\theta) = I^{(s)}[\beta(\theta)] \quad (1.11)$$

where $I^{(s)}(\beta)$ is the surface brightness function in the source plane and $I(\theta)$ is the surface brightness function in the image plane. The brightness function in the image plane is likely to be very different from that in the source plane, therefore a way of quantifying this distortion is needed. If the extent of the source is small enough that over its entire surface, the characteristics of the lens distorting it do not change then the extent of the distortion may be expressed using a Jacobian matrix

$$A(\theta) = \frac{\partial\beta}{\partial\theta} = \left(\delta_{ij} - \frac{\partial^2\psi(\theta)}{\partial\theta_i\partial\theta_j} \right) = \begin{pmatrix} 1 - \kappa - \gamma_1 & -\gamma_2 \\ -\gamma_2 & 1 - \kappa + \gamma_1 \end{pmatrix} \quad (1.12)$$

The two elements γ_1 and γ_2 are components of the quantity known as the shear which in total is represented as

$$\gamma = \gamma_1 + i\gamma_2 = |\gamma|e^{2i\phi} \quad (1.13)$$

This yields the two components of image distortion in a lensing system. The uniform magnification due to the density of the lens represented by κ and the anisotropic magnification (ie. distortion) due to the local shear represented by γ may in total be represented by

$$\mu = \frac{1}{\det A} = \frac{1}{(1 - \kappa)^2 - |\gamma|^2} \quad (1.14)$$

This quantity may be either positive or negative representing the polarity of the image with absolute values less than 1 representing demagnifications and values greater than 1 representing magnifications. [13].

In astrophysical observations, there is no prior knowledge about the brightness or shape of the background sources and it is only the shapes of the images which may be measured. In this situation, only a relative distortion may be calculated which maps from one image onto another, not an absolute distortion mapping from the source to the image plane.

1.2 Weak Lensing

The main investigations in this report are primarily concerned with the phenomenon of weak lensing where multiple images are not observed. The principles described here still hold true but there are no multiply imaged systems to constrain the mass model [1]. In order to map the mass distribution using weak lensing, a quantity called the 'reduced shear' is measured. This quantity is defined by

$$g = \frac{\gamma}{1 - \kappa} = \frac{|\gamma|}{1 - \kappa} e^{2i\phi} \quad (1.15)$$

and the associated magnification matrix is

$$A(\theta) = (1 - \kappa) \begin{pmatrix} 1 - g_1 & -g_2 \\ -g_2 & 1 + g_1 \end{pmatrix} \quad (1.16)$$

where g defines the anisotropic stretching of the image (ie. shape distortion) and κ defines the isotropic magnification of the image.

Weak gravitational lensing analysis relies not on measuring the distortions in the images of single background sources but rather in finding the statistical bias towards preferentially oriented images over a large sample of weakly sheared background sources. Unlike strong lensing, observation of any single background source galaxy is not sufficient to establish the presence of weak lensing. The fact that background galaxies are randomly oriented on the sky is by far the dominant effect in single cases and small samples and almost completely overrides the contribution to source galaxy shape by weak shear. In order to detect the presence of weak lensing, a large sample of background sources is required. Very accurate measurement of the shapes of these sources is needed in order to establish both the ellipticity of the source and its orientation on the sky. With this data for the large sample, an average image polarisation as a function of distance from the lens can be calculated, this is the weak shear profile. The weak shear is measured as two components. The first, the tangential shear is a measure of the tendency of source images to be aligned tangentially to the lensing potential and is expressed as

$$\tau_t = \sum_i \epsilon_i \cos 2\phi_i \quad (1.17)$$

Where ϵ_i and ϕ_i are the ellipticity and orientation of a given galaxy, i . A positive value for tangential shear represents the detection of a tendency in the images to be aligned tangent to

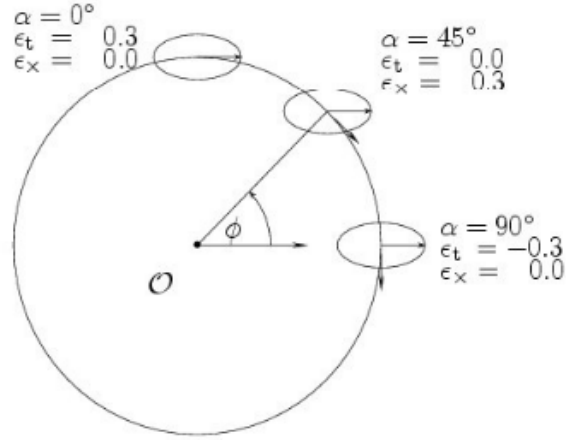


Figure 1.2: The contribution of different source galaxy orientations to the components of the weak shear signal

the lens, the more positive the value. The stronger this tendency becomes. It is also possible for tangential shear to take on a negative value. In this case, the physical significance of such a value is the detection of a tendency for images to be *radially* aligned to the lens.

The second component is the cross-component of the shear and is treated as a measure of the occurrence of systematic error in the signal detection. It is expressed as

$$\tau_x = - \sum_i \epsilon_i \text{Sin}2\phi_i \quad (1.18)$$

In order for a reliable detection of a weak lensing signal to be confirmed, it is important that the cross component of the shear be consistent with zero for each value of the tangential shear.

A diagrammatic representation of the contribution of several different background galaxy orientations to the two components of the shear is presented in Figure 1.2.

1.3 Previous Work in this Field

1.3.1 The Development of Galaxy-Galaxy Weak Lensing

Measurements of weak gravitational lensing signals became possible with the advent of deep survey imaging using CCDs. [29] Although the majority of early work on gravitational lensing involved the study of background galaxies that had been magnified and distorted by their light's distortion by massive galaxy clusters [10], a large proportion of the remainder of this report concerns the phenomenon of weak gravitational lensing. Deep survey imaging has allowed resolution of very faint background galaxies both in the field and with intervening galaxy clusters. It has been shown [8] that in order to fully map the mass distribution of a cluster, the contribution to the shear from individual galaxy halos in the cluster and not just the smooth cluster potential must be taken into account.

The majority of the existing work on Galaxy-Galaxy weak lensing concerns galaxies in the field and has not given treatment to the study of the phenomenon in a cluster environment.

The first detection of galaxy-galaxy weak lensing by Brainerd, Blandford and Smail (1996) [2] claimed a 1% detection of the weak shear signal at the 3σ level. This investigation was carried out on a large population (≈ 10000) of background source galaxies in the field with a magnitude range between 23 and 26 in the r-band. Each of these galaxies was then paired with a foreground galaxy that was close on the sky. The signal was detected in this case by looking for polarisation of the image of each source galaxy in the sample and then averaging over the whole galaxy sample. The result of this averaging was a signal suggesting a 1% preferential tangential polarisation of source galaxy images. In order to test the robustness of this result, the authors then went on to construct a Monte-Carlo simulation to ray-trace a simulated source population by a population of simply modelled field galaxies. The simulation was simplified by the adoption of a singular mass-model for the field galaxies as the study was explicitly uninterested in the central regions of its field galaxy population (to the extent of excluding the central 5 arc-seconds of the galaxy lens from the analysis). The simple profile adopted by the foreground galaxy population was expressed as

$$\rho(r) = \frac{V_c^2 s^2}{4\pi G r^2 (r^2 + s^2)} \quad (1.19)$$

The faint background population was generated with random orientations and their red-shift was scaled by their randomly assigned luminosity. With the use of these populations and many iterations of the Monte-Carlo simulation, a good first approximation to the halo parameters was made. By χ^2 minimisation, the best-fit parameters for the halos was determined. The galaxy-galaxy simulations yielded results that were consistent with those obtained through observation which gave strength to the notion that the observed signal was, in fact, astrophysical in origin.

The detection of weak lensing is, by its nature, a difficult process. A signal of the order 1% can be easily concealed within the noise of the random ellipticity distribution of the source galaxies under examination. The process is also prone to false signal detection due to systematic errors during measurement. To test against these errors, Brainerd, Blandford and Smail looked at the possible contribution to the signal from an elliptical point-spread function in their imaging data. They also considered the possibility that objects near the foreground galaxies that had been assumed to be faint background galaxies were in fact dwarf companions of the foreground galaxies whose elongation was due to a tidal interaction with their giant companion. It was discovered that the contribution of dwarf companion elongation to their measured shear signal was around 2.3σ below the measured signal and was not, therefore, the source of the signal. With the measurement process showing no signs of systematics and contributions to the shear signal from other sources mentioned previously, the signal was determined to be physical in origin and the first reliable detection of background galaxies being lensed by foreground galaxies.

1.3.2 Studies of Galaxy-Galaxy Weak Lensing in Cluster Cores

The work of Brainerd, Blandford and Smail was built on by Natarajan and Kneib in 1997 [16] who expanded the examination of weak galaxy-galaxy lensing into galaxy cluster environments. The original work was purely based on simulations conducted to assess the viability of galaxy-galaxy weak lensing signal detection in a cluster environment. The major original aim of utilising galaxy-galaxy weak lensing in clusters was to detect the presence and extent of dark matter subhalos within the cluster. As had been shown [8] in order to reliably model and reconstruct the mass distribution within a cluster, a knowledge of the substructure mass function, a measure of the frequency of occurrence of dark halos per mass interval, is crit-

ically important. Although previous work by Jean-Paul Kneib [8] had previously mapped mass distribution at large clustercentric radii, the presence of substructure in the galaxy-galaxy lensing signal had been effectively masked by the large smoothing lengths used in that work. The work of Natarajan and Kneib sought to reveal the effect of substructure on the lensing signal by use of higher resolution methods. A reliable measure of dark matter subhalo masses and radii would allow constraints to be put on the substructure mass function within the cluster. The substructures in question are assumed to be present in the outermost regions of bright cluster galaxies within a large cluster of galaxies where it may take the form of low luminosity satellite galaxies or dark matter halos with no luminous baryonic matter component. The assumption made in the study of galaxy-galaxy weak lensing is that light traces mass. This hypothesis had long been employed in weak lensing studies but was further motivated by work performed by Wilson et al in 2001 [32] for field galaxies and Clowe et al in 2002 [4] in cluster environments.

Natarajan et al 1997 [16] also derived scaling relations for use with their cluster galaxy modelling. The cluster galaxies were modelled using a Truncated Pseudo-Isothermal Elliptical Mass Distribution (described in Kneib 1996 [8]) with relevant parameters (Central velocity dispersion, Truncation radius and core radius) scaled by luminosity. Truncation is achieved by the superposition of two PIEMD components as shown below.

$$\Sigma(x, y) = \Sigma_o \frac{r_{core} r_{cut}}{r_{cut} - r_{core}} \left(\frac{1}{\sqrt{r_{core}^2 + \rho^2}} - \frac{1}{\sqrt{r_{cut}^2 + \rho^2}} \right) \quad (1.20)$$

where

$$\rho = \frac{x^2}{(1+e)^2} + \frac{y^2}{(1-e)^2} \quad (1.21)$$

Adoption of a maximum likelihood analysis of the subhalo velocity dispersion and halo radius allowing them both to be constrained independently (as opposed to the direct averaging method used in the original work in this report) in regions where the smooth cluster potential varies over the scales under consideration. Using these methods, a strong galaxy-galaxy lensing signal was detected within the simulated clusters at the 5-10% level suggesting that the signal receives a significant boost from the effect of the smooth cluster potential (earlier work by Kneib et al had detected a 1% signal in the field). Subsequent investigation in this paper further developed the viability of galaxy-galaxy lensing in cluster environments by identifying that the maximum shear signal was obtained when the lensing cluster was at a redshift of 0.2. In conclusion, the paper determined that galaxy-galaxy lensing was applicable for galaxy cluster environments based on a minimum of 20 stacked HST WFPC2 frames which are required to reduce the noise intrinsic to the ellipticity distribution of source galaxies.

Further development of galaxy-galaxy weak lensing in clusters was made by Natarajan et al. (1998) [19] who took the suggested methods from earlier work [16] and applied them to the lensing cluster AC114 located at redshift 0.31. Use of these methods showed that for an L* cluster galaxy, the majority of the galaxy mass was contained within a radius of 15kpc with an approximate mass-to-light ratio of 15. When compared to earlier work conducted on field galaxies, these results suggested that the dark matter halos surrounding cluster galaxies were substantially less massive and extended than those of field galaxies measured using lensing techniques. They also observed that the efficiency of tidal stripping by the cluster potential varied with galaxy type, typically finding that S0 galaxies were the least extended. At the time, comparison with results from the field was difficult as an optimum sample of field galaxies was not available for detailed comparison. This was

somewhat resolved by Ebbels (1998) [6] which featured a search for a weak lensing signal due to field galaxies in an archival Hubble Space telescope dataset. This thesis also measured the distribution of background galaxy ellipticities and fitted a model to the distribution which, to first order, showed that background galaxies are randomly oriented on the sky.

Due to the importance of understanding the prevalence of substructure within a cluster to cluster evolution, the paper suggested that this method be expanded to include a larger sample of galaxy clusters than the single cluster presented in 1998 in order to better understand the prevalence and implications of substructure in rich clusters. This paper also predicted the usefulness of the then upcoming ACS instrument aboard the HST to future galaxy-galaxy weak lensing studies.

The analysis described previously was expanded by Natarajan and Kneib (2002) [17] which this time contained the weak lensing results from a variety of massive cluster lenses between redshifts of 0.17 and 0.58. In total, 5 clusters were examined. Again using the cluster galaxy scaling relations derived in the 1997 paper, [16] the parameters of an L^* cluster galaxy were described. Taking results across all the clusters that were examined, it was estimated that the cluster galaxy perturbers within the smooth cluster host potential contributed between 10% and 20% of the total cluster mass, strongly suggesting that the majority of dark matter within a massive lensing cluster is smoothly distributed. In a further development of an observation made in the earlier Natarajan 1998 paper, [19] it was detected to a 3σ level that the dark matter halos of cluster galaxies are substantially truncated due to tidal stripping by the cluster potential. Encouragingly, these results appear to agree well with the predictions of tidal truncation theories. Dark matter halos as large as those observed around galaxies in the field were very strongly excluded to a 10σ level, demonstrating a large difference between halos in different environments.

A further development in the use of weak lensing in cluster environments was demonstrated in Natarajan et al.(2002) [20] which investigated the nature of dark matter itself. Observations made of the rich lensing cluster Abell 2218 allowed constraints to be put on the truncation radii of dark matter subhalos within the main cluster potential. It was found to a 5σ level that the extent of these truncated dark matter halos agreed with the predictions of the theory of collisionless dark matter. The truncation radii were found to be inconsistent with models including ram pressure stripping of dark matter material effectively excluding the theory that dark matter is, in fact, a strongly interacting fluid.

Natarajan and Springel (2004) [21] compared the results from the archival HST weak lensing observations from Natarajan et al 2004 [18] with N-body simulations designed by Volker Springel. The study found a strong agreement between the observed and simulated results for the substructure mass function in the mass interval $10^{12.5} - 10^{11} M_{\odot}$. (ie. Cluster galaxy scale dark matter halos). The degree to which the observations and simulations agree is exemplified by the fact that no free parameter fitting or scaling was used to obtain the observational fit to the simulation data. A prediction of the N-body simulations however is that there should be a significant portion of the substructure mass function with masses below $10^{11} M_{\odot}$ which are currently not detectable by galaxy-galaxy weak lensing measurements. Current weak lensing techniques therefore are able to detect the majority of the mass contained within substructures but only a small fraction of the total number of substructures. Despite good agreement over the mass range described, there is a possible overprediction of the occurrence of more massive ($> 10^{12.5} M_{\odot}$) substructures by the simulations although the author notes that this phenomenon could equally be due to an underestimate by the lensing methods employed in the paper.

Development of the ideas put forth in Natarajan (2002) [17] and (2004) [18] was presented in Natarajan, DeLucia and Springel (2007) [15] where the substructure mass

function was sought to provide a test of hierarchical galaxy formation theory. The paper was motivated by Moore et al (1999) [7] which identified a discrepancy between observation and simulation for small satellite galaxies in orbit around the Milky Way. Simulations predict a factor 2-3 more dwarf galaxies in orbit around a galaxy of the size of the Milky Way. Detection had focused on finding luminous baryonic matter in these dwarf galaxies which traced the dark matter distribution, however, hypotheses put forward by Bullock et al (2000) [3] suggest that due to suppression of gas accretion after the epoch of reionization, star formation in low mass halos is significantly reduced. A low star formation rate in low mass halos means that such halos have a very high mass-to-light ratio and are therefore most likely to be detected by perturbing effects on weak shear maps of the outer regions of galaxy halos. This deficiency is not expected to affect studies of clusters as strongly as the study of field galaxies since the majority of cluster subhalos have a significant luminous baryonic component (although it is assumed that for substructures within these subhalos, a similar problem may arise although these substructures only contribute a small amount of the total cluster mass). The characteristics of cluster galaxy perturbers within a cluster environment were found to be largely independent of the mass model chosen to represent the smooth cluster potential. Utilising a maximum likelihood method to find the most probable perturber parameters led to the conclusion that 10-20% of the total cluster mass was present in the form of truncated galaxy-scale dark matter halos to 3σ accuracy. This paper also performed a rigorous test on the methods used for detecting the notoriously weak galaxy-galaxy signal by altering the simulations in several ways designed to disrupt the detected signal. Perturbing cluster galaxies were moved to random positions in the simulated clusters and perturber-centric shear measurements were made. Reassuringly for the method, this disruption produced nothing but noise on the 2-dimensional likelihood surfaces used to extract the most likely parameters, further strengthening the evidence that the observed signal is indeed due to galaxy-galaxy lensing.

Galaxy-galaxy weak lensing has been shown to be capable of probing the distribution of substructure in cluster environments down to around $10^{11} M_{\odot}$ (or approximately 10^{-4} of the total host halo mass. As suggested by Taylor and Babul, [28] the study of galaxy evolution requires information about substructures of even lower fractional mass than this. Further refinements to the study of galaxy-galaxy weak lensing will therefore be required in order to apply it to future tests of CDM physics.

1.3.3 Galaxy-galaxy Weak Lensing Beyond Cluster Cores

Galaxy-galaxy lensing techniques were employed in Limousin et al 2007 [11] using a maximum likelihood method to constrain the cluster galaxy halo parameters. The study was able to probe cluster galaxies in a range of environments from the cluster core out to around 2Mpc using wide-field ground based data on the CFH12K instrument. Their findings supported conclusions made from numerical simulations with those cluster galaxies closest to the cluster centre having significantly more truncated dark matter halos than those closer to the cluster edge. The maximum likelihood method gave truncation radius values of around 50kpc (compared to several hundred kpc in field galaxies) which, when coupled with aperture masses obtained by weak lensing analysis, demonstrated that massive galaxies in cluster environments have lower halo masses and a more truncated halo extent than galaxies of similar morphology in the field.

The strength of unifying weak and strong lensing to constrain the mass distribution of a galaxy cluster was shown in a study of the massive cluster Abell 1689 by Limousin et al in 2007 [12] where knowledge of the mass profiles of individual cluster galaxies combined with strong lensing redshift constraints allowed for one of the most comprehensive lensing

based reconstructions of a massive galaxy cluster to date. Galaxy-galaxy weak lensing has potential to offer more accurate reconstructions of the mass profile of individual cluster galaxies than ever before. Limousin showed in his previously mentioned paper on dark halo truncation in clusters that galaxy-galaxy weak lensing was able to identify the tidal stripping of galaxy-scale dark matter halos by identifying upper limits to their cut radius parameter. With increasingly available high resolution datasets it is possible that using this technique, substructure information of increasing accuracy may be included in whole cluster studies to more reliably constrain their mass.

A more recent study by Natarajan, Kneib and Limousin [14] took the use of galaxy-galaxy weak lensing techniques in clusters a stage further by examining the effect of tidal dark matter stripping in three radial bins of clustercentric radius. This allowed conclusions to be drawn not just on the effects of tidal stripping on cluster galaxies as a whole but rather an (albeit fairly low resolution due to only having 3 radial bins) evolutionary history of the stripping of galaxies as they fall deeper into a cluster potential. This study on HST imaging of the cluster Cl0024+16 found, using similar techniques described in Limousin 2007, that there seems to be a positive correlation between mass and halo extent with clustercentric radius (i.e. galaxies become both less massive and more compact closer to the centre of the cluster potential) but that tidal stripping efficiency was lower than that suggested in simulations. By looking at a larger sample of clusters with similar image quality and established scaling relations, it would be my hope that an increased number of bins of clustercentric radius could be used for a similar investigation while maintaining the number density of foreground/background galaxy pairs critical for detecting a galaxy-galaxy weak lensing signal.

The increasing number of large-scale surveys allows for an unprecedented expansion of the study of galaxy-galaxy weak lensing. With a greater number of clusters available for analysis, the lower end of the cluster mass function can be probed allowing a study of halo stripping as a function of not only clustercentric radius but of environment. The most recent cluster sample of this type that will form the motivation and core data for weak lensing measurements in this report comes from the work of Okabe et al, [23] a study of 30 massive galaxy clusters using the Subaru SuprimeCam instrument.

1.4 New Observations

LoCuSS (Local Cluster Substructure Survey) is a large, multi-wavelength collaboration first motivated by the paper by Smith et al. (2005) [25] which performed a comprehensive study on the cluster core morphology in a sample of ten galaxy clusters at a redshift near $z=0.2$. Through use of a wide selection of multi-wavelength data, the LoCuSS survey aims to determine the impact of cluster dynamical state on the shape of its mass-observable scaling relations and the impact, if any, that cluster assembly history has on the cooling of the hot X-ray emitting gas within the cluster core.

Smith et al. (2005) was the first to study cluster cores with a combination of high resolution space-based (HST WFPC2) imaging and high quality X-ray observations from the Chandra observatory. The union of these superbly detailed data sets allowed the study to conclude both that the majority of the X-ray selected clusters were unrelaxed having undergone (or in the process of undergoing) major mergers and that the scatter in the Mass X-ray temperature relation, an important concept in using galaxy clusters as a cosmological probe, was much higher than was previously measured (by a factor of 3) These findings motivated the LoCuSS survey to try to better understand the issues involved in using massive galaxy clusters as probes of cosmology. The sample used in Smith et al 2005 is known as the

LoCuSS pilot survey and is the sample chosen for the galaxy-galaxy weak lensing analysis described later in this report. This study detected significant differences between the mass-temperature relations of relaxed and unrelaxed (or disturbed) clusters within the sample which exceeded the expected theoretical predictions for differences in these parameters by up to a factor of 3.

LoCuSS has collected multi-wavelength data on 100 massive clusters at intermediate redshift. With this unprecedentedly rich dataset, a logical expansion of the studies described in the literature to a much larger cluster sample becomes possible which should allow a more robust constraint to be put on the substructure mass function in cluster environments. Currently existing data includes optical cluster observations from the Hubble space telescope which may then be followed-up spectroscopically by large ground-based telescopes such as VLT and Keck in order to constrain the redshift of strongly lensed arcs. On the weak lensing side, data from the Subaru telescope SuprimeCam instrument allows wide field ($34' \times 27'$) cluster imaging for the probing of the cluster shear signal and cluster substructure out to the infall region (around twice the virial radius) of a cluster at a high effective resolution of $0.2''$ per pixel. These data are complimented by X-ray observations from XMM-Newton and Chandra which measure the core cluster mass by mapping the distribution of luminous X-ray emitting gas.

1.4.1 This Thesis

The aim of this thesis is to examine the phenomenon of galaxy-galaxy weak lensing within these massive galaxy clusters including an assessment of the feasibility of detection with currently available data. In addition to this, it will aim to verify or otherwise, untested assumptions that were made during the process of retrieving the shape information which is key to the measurement of this extremely weak effect.

The structure of the remainder of this thesis will be as follows. Chapter 2 will analyse HST galaxy shape information in a sample of 10 X-Ray selected clusters and attempt to measure a galaxy-galaxy shear signal as a function of foreground/background galaxy pair separation. Chapter 3 Will detail the simulations constructed to measure the systematic effect of poor subtraction of the cluster-scale shear signal from a catalogue of background galaxies. Chapter 4 will explain the process of designing telescope masks for follow-up observations of massive clusters to obtain spectroscopic redshifts for instruments on two large optical telescopes (Gemini GMOS and VLT FORS). Chapter 5 will detail conclusions drawn from the investigations in the previous chapters.

Chapter 2

Galaxy-Galaxy Weak Lensing

This chapter will attempt to measure the galaxy-galaxy weak lensing signal from a previously published [25] X-Ray luminosity selected sample of ten massive galaxy clusters. The cluster cores in this sample have multi-wavelength constraints which, together with their X-Ray selection allows the comparison of galaxy-galaxy weak lensing signals in cool core and non-cool core clusters.

2.1 Data and Analysis

The object catalogues used for this analysis were derived from imaging taken with the Hubble Space Telescope WFPC2 instrument of the ten galaxy clusters that form the LoCuSS pilot survey [25]. The superior image quality afforded by the WFPC2 instrument allows for unprecedented accuracy in shape measurement for the population of faint background galaxies. Cluster mass component parameters used in this investigation are detailed in Table 2.1. In all a total of 20 catalogues were considered, one catalogue of foreground cluster galaxies and one of faint background galaxies for each of the ten clusters in the sample. The cluster sample comprised seven unrelaxed or disturbed clusters, namely Abell 68, Abell 267, Abell 773, Abell 1763, Abell 2218, Abell 2219 and Abell 209 and three relaxed clusters, Abell 383, Abell 1835 and Abell A963. Although this sample data has highly precise shape measurements due to the high resolution of the instrument, (0.05 arcseconds per pixel after drizzling) the frames from which the data were derived are only 3 arcminutes in width. At a redshift of 0.2, the approximate redshift of each of the clusters in the sample, this corresponds to a cluster radius of 500kpc, only a third to a half of the cluster virial radius. This effectively limits the relevance of this part of the study to the regions of the cluster core meaning the result will not be general for all cluster environments. The catalogues contained the X and Y frame coordinates of each cluster and background galaxy (with the Bright central Galaxy or BCG of each cluster taken to be at (0,0)) along with the apparent magnitude of each. Also included was a measure of both the semi-major and semi-minor axes of each galaxy and that galaxy's angular orientation.

Cluster	Component	$\Delta R.A.$ (arcsec)	ΔDec (arcsec)	Axis ratio (a/b)	θ (Deg)	r_{core} (kpc)	r_{cut} (kpc)	σ_0 (km s^{-1})
A 68	A	0.6	-0.7	2.2	37	108	1000	950^{+10}_{-10}
	B	-45.8	68.4	1.0	58	81	1000	707^{+20}_{-20}
	BCG	-0.2	0.0	1.7	37	0.3	83	301^{+10}_{-10}
A 209	A	0.0	0.0	1.9	43	50	1000	630^{+20}_{-100}
A 267	A	0.0	0.0	2.0	-60	115	1000	1060^{+40}_{-40}
A 383	A	0.3	0.5	1.13	109	51	1000	900^{+10}_{-10}
	CGal A	14.9	-16.8	1.13	-7	2.2	40	176^{+10}_{-10}
	BCG	-0.5	0.1	1.07	126	0.6	110	310^{+30}_{-20}
A 773	A	0.0	0.0	1.9	-38	75	1000	750^{+60}_{-70}
	B	1.0	24.0	1.8	-10	75	1000	700^{+70}_{-100}
	C	84.4	12.0	1.0	...	75	1000	550^{+75}_{-150}
A 963	A	0.0	0.0	1.7	90	95	1000	980^{+15}_{-15}
	BCG	0.0	0.0	1.1	90	2	96	320^{+15}_{-15}
A 1763	A	0.0	0.0	1.9	180	70	1000	700^{+20}_{-150}
A 1835	A	0.0	0.0	1.5	70	70	1000	1210^{+80}_{-100}
A 2218	A	0.2	0.5	1.2	32	83	1000	1070^{+5}_{-5}
	B	47.0	-49.4	1.4	53	57	500	580^{+15}_{-15}
	CGal A	16.1	-10.4	1.1	70	2	65	195^{+10}_{-10}
	CGal B	4.8	-20.9	1.4	-23	2	77	145^{+10}_{-10}
	BCG	0.3	0.1	1.8	53	3	136	270^{+7}_{-7}
A 2219	A	0.1	0.2	1.7	35	77	1000	902^{+10}_{-10}
	B	39.2	-32.0	1.1	8	55	375	515^{+10}_{-10}
	C	-22.9	4.5	1.0	...	31	365	395^{+20}_{-20}
	BCG	0.0	0.0	1.6	29	3	120	278^{+10}_{-10}

Table 2.1: The parameters of modelled mass components for each of the ten clusters examined in this section. Taken from Smith et al (2005) [25] The table features mass components of cluster, group and individual bright galaxy scales, as indicated in the second column.

The weak lensing analysis was, in this case, not interested in the shear induced in the background galaxy images by the bulk mass component of the cluster but only by the shear from individual cluster galaxy dark matter halos. In order to ensure that only the galaxy dark matter halos contributed to any measured signals, it was necessary for the cluster component shear contribution to be subtracted from the original catalogues. Models for the cluster potential were taken directly from the values fitted to the clusters including central velocity dispersion and cluster core radius. These parameterised mass distributions comprise one or more cluster or group-scale dark matter halos plus the few cluster galaxies massive enough to contribute significant cluster substructure (down to a limiting magnitude fraction of $L^*[25]$). We used the Lenstool software to generate a 25x25 grid of shear values across the cluster frame out to a radius of around 90 arcseconds from the cluster centre. To subtract the cluster contribution from the catalogue, each background source was matched with the nearest (based on X,Y coordinates) cluster shear value in the grid. Using the magnitude and orientation of the shear, the ellipticity was decomposed into semi-major and semi-minor components and vectorially subtracted from the semi-major and semi-minor axis values in the catalogue. An example of the shearmaps generated for the clusters can be seen in Figure 3.1. This shearmap is for a simple single component halo model for the cluster A383.

Subtraction of the cluster signal from the catalogues left only two contributions to the observed source galaxy shapes, the random distribution of galaxy ellipticity and lensing by individual galaxy-scale dark matter halos. The task was to isolate the lensing signal from the much stronger random ellipticity noise. A further problem was found to be that source galaxies situated close to the cluster centre were in the strong lensing regime. This meant that the sources close to the centre had their shape distorted by multiple halos which was found to add too much noise to their shear values. To combat this, it was decided that those source galaxies within the central 40 arcseconds, typically twice the Einstein radius of the cluster, of each cluster were to be excluded from the foreground-background pairing.

The orientation of the source galaxy with respect to the paired foreground cluster galaxy was represented as ϕ where

$$\phi_i = \text{Tan}^{-1} \left(\frac{yf_i - yc_j}{xf_i - xc_j} \right) - \theta_i \quad (2.1)$$

where xf_i and yf_i are the x and y coordinates of the background galaxies and xc_j and yc_j are the x and y coordinates of the cluster galaxies. With the orientation and separation of each pair, the last value needed for the calculation of the shear components was the ellipticity, in this case defined as

$$\epsilon_i = \frac{a_i^2 - b_i^2}{a_i^2 + b_i^2} \quad (2.2)$$

where a_i and b_i are the measured semi-major and semi-minor axes of a background galaxy's ellipticity.

The final calculation was the use of equations 1.18 and 1.19 to obtain values for the tangential and cross component of the shear for each pair.

In order to generate a shear profile based on the calculated values, a suitable binning by pair separation was chosen. A bin width of 2 arcseconds with a 1 arcsecond oversample was found to give the best results. Each cluster catalogue contained the order of 50 cluster galaxies and 500 background source galaxies resulting in around 25000 possible galaxy-galaxy pairs for each cluster. The noise from the random ellipticity distribution was found to be so pronounced that shear profiles for single clusters were dominated by noise motivating the signal from all ten clusters used in the investigation to be stacked to obtain a single average profile which would show any general trends in galaxy-galaxy shear within clusters. Using

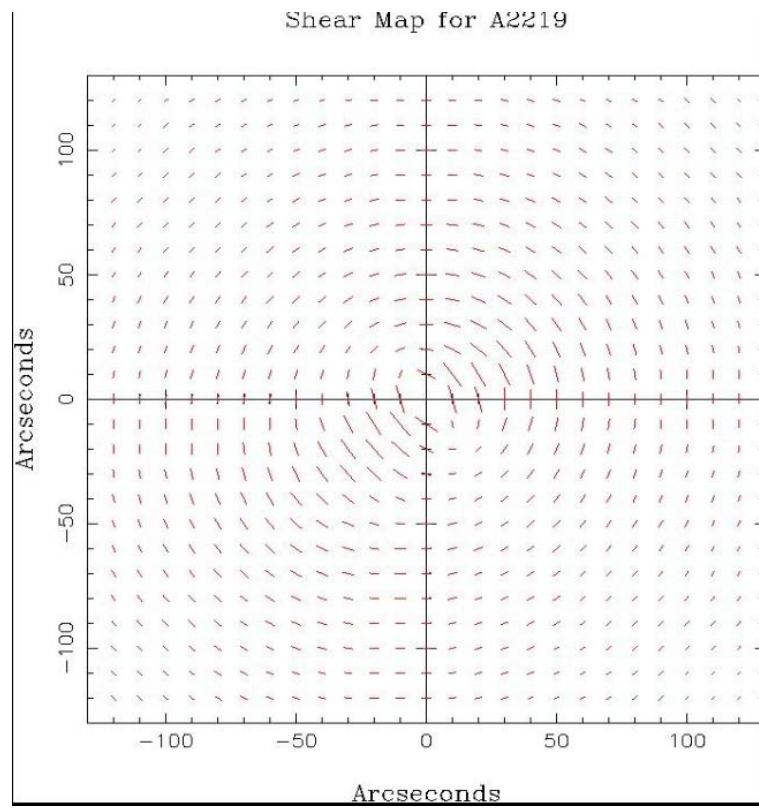


Figure 2.1: Generated shear map showing the magnitude and direction of the weak shear caused by the cluster potential. In this example, the map is for the cluster A2219.

250000 galaxy-galaxy pairs and binning the data as described previously, a signal to noise ratio of 6 was achieved for the shear measurement across all ten clusters (See Figure 2.2).

The measurement of error on the value of tangential shear was subject to considerable error. The magnitude of the error was given by σ/\sqrt{n} where σ was the standard deviation of the measured shear values in each separation bin and n was the number of foreground-background galaxy pairs within each bin. The lensing signal scaled with n while the error scaled with the inverse of \sqrt{n} making the number of galaxies in each separation bin critical to measuring the shear reliably. At low separation values, there were only of the order 5-10 galaxies in each bin so the magnitude of the error was of the order of the magnitude of the signal. With this in mind, the values in the first 4 arcseconds or so of the profiles is generally subject to a much greater error than bins for larger pair separations where the number of pairs in each bin was of the order of 1000. In certain clusters, some of the innermost bins contained no galaxy pairs, in this case, the bin was excluded from the profile plot. Shear profile plots generated by this method are presented in a following discussion section.

2.2 Results and Discussion

The application of the methods described in the previous chapter to the sample of 10 clusters yielded interesting results when the galaxy-galaxy shear contributions from all ten clusters were added together and binned by pair separation similar to the work of Natarajan et al [16]. In figures 2.2 to 2.6, the Y-Axis value ' E_{tan} ' represents the measured value of the shear signal with a value of 0.1 representing a 10% tendency for background galaxies to be aligned tangent to the cluster centre. The investigation was focused to look at the weak shear profile on small scales. The result of this was Figure 2.2 which shows the shear profile averaged over all ten of the sample clusters for pair separations between 0 and 20 arcseconds. As expected, this plot shows large error on the central shear values due to there being so few galaxy-galaxy pairs at such low separations with the error bars steadily decreasing in magnitude as the separation (and so the number of galaxies in each bin) increases. A look at the cross component of the shear in Figure 2.2 (open points) shows that they are generally consistent with zero across the profile which increases confidence that systematic errors are not present in the analysis.

In general agreement with Natarajan 1997 [16], the profile shows that the weak tangential shear signal is largest when the pair separation is low and although the magnitude of the shear does not reach the 20% values predicted by the Natarajan simulations of a cluster with $z=0.2$, the general trend of the shear value decreasing out to larger radii is in good agreement. The significant difference from the currently published observations is the profile feature that exhibits at separation scales around 15 arcseconds where a significant bump may be seen.

Initially thought to be an aberration induced by the inclusion of clusters with only weak lensing constraints on the cluster mass distribution (which leads to poor constraints on the cluster signal compared to those clusters which also have strong-lensing constraints from multiple images), a first attempt to identify the source of this 'bump' was made by splitting the ten cluster sample into two groups, one with strong lensing constraints and one without. This divided the sample into two groups of five clusters each. The profile generating script was run once on each of these groups. The results of this are demonstrated in Figure 2.3, which shows the shear profile for only those clusters with strong constraints and Figure 2.4 which shows the profile for clusters with only weak constraints. It was found that the clusters with strong lensing constraints did not exhibit the well-behaved shear profile that was predicted, with only the weakly constrained cluster group showing anything like the

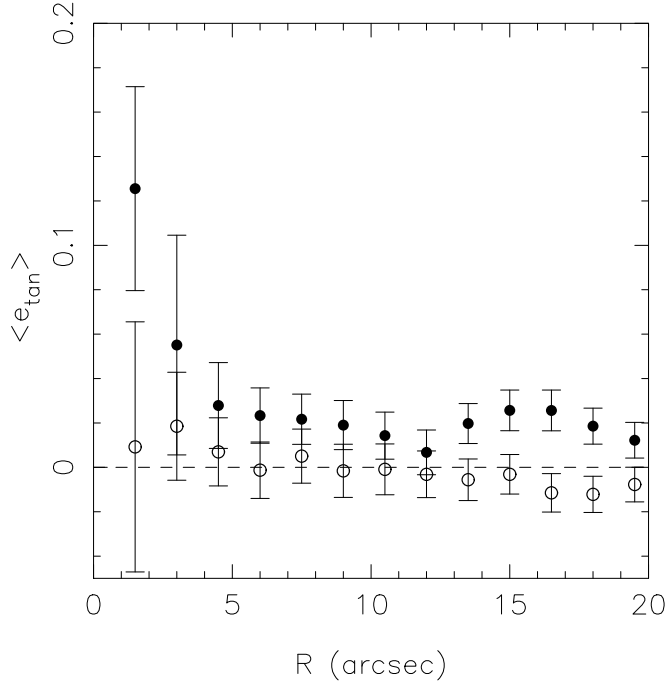


Figure 2.2: Weak shear profile of the ten stacked pilot clusters

result obtained when stacking all ten clusters. It should be noted that the larger scatter on the points in the weakly constrained plot (Figure 2.4) is primarily due to a twofold reduction in the number of pairs in each bin due to half the sample being excluded in this test. The results of this test were inconclusive with the weakly constrained plot still showing some signs of the anomalous feature at 15 arcseconds.

In order to further investigate the origins of the feature, the sample was again split, this time into those clusters that were most relaxed and those which were least relaxed defined by the offset between their modelled mass peak and the observed peak location of X-ray emission. Again the profile generating script was run on these two groups. The results are displayed in Figure 2.5 which shows the profile for those clusters that were most relaxed and Figure 2.6 which shows the profile for less relaxed clusters. This time, the result is far more clear-cut with the relaxed clusters exhibiting the predicted well-behaved shear profile with the magnitude of the tangential shear decreasing as pair separation increases while the unrelaxed plot shows both a radially decreasing shear profile coupled with a more pronounced version of the 15 arcsecond feature. The feature therefore, appeared to be unique to those clusters in the sample that were most disturbed. It was noted that the most disturbed clusters had a significant proportion of the cluster mass, that of the intracluster gas, offset from the main potentials detailed in Smith et al 2005. It was thought that at the stage of subtracting the contribution to the shear from the smooth cluster potential, not taking this offset gas mass contribution into account could have left a residual effect on the final shear profile and so an attempt should be made to remove its contribution as well. The offsets for each of the gas potentials were documented in Smith et al 2005 so using these values, a further potential was added to the lenstool model. For each cluster, the mass contribution this 'gas potential' contributed to the total cluster mass was varied from 10% up to 50% of the total mass to see what effect this would have on the shear

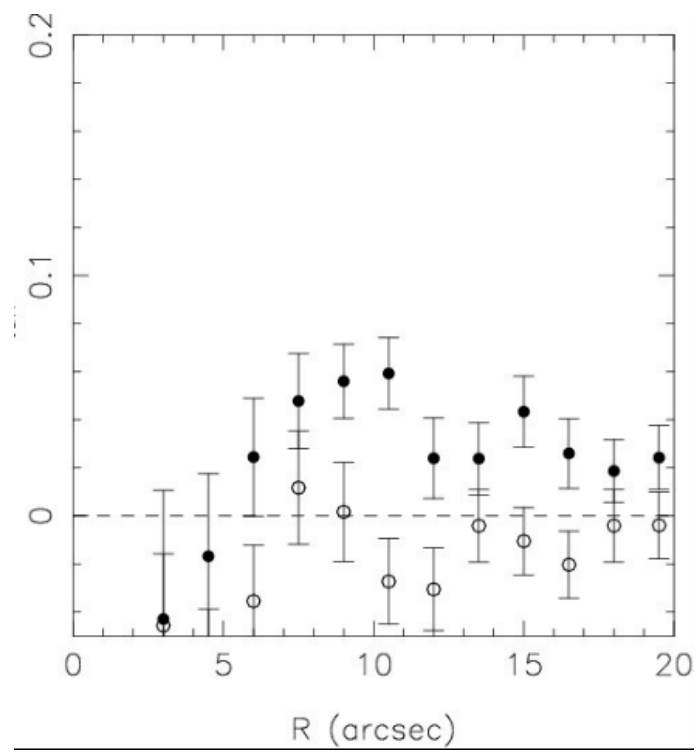


Figure 2.3: Weak Shear profile for the five stacked clusters with strong lensing constraints.

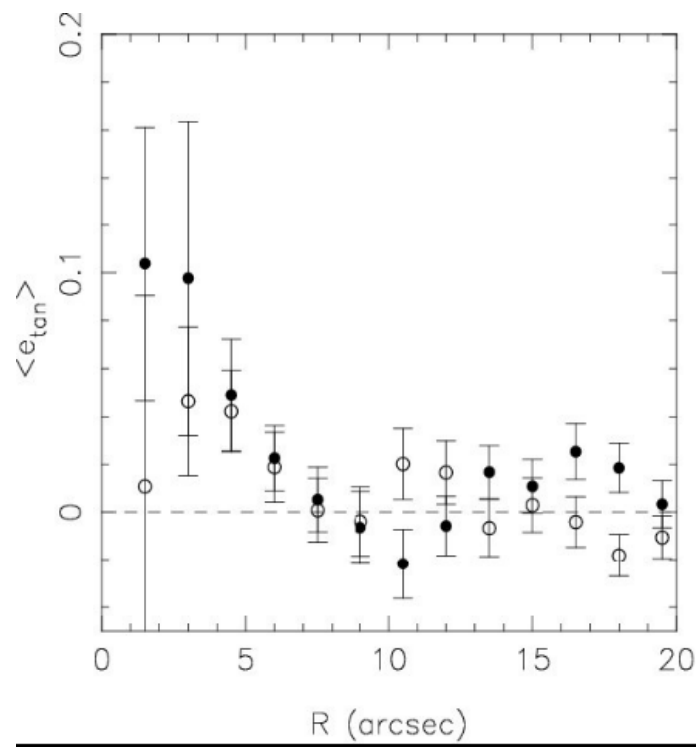


Figure 2.4: Weak Shear profile for the five stacked clusters without strong lensing constraints.

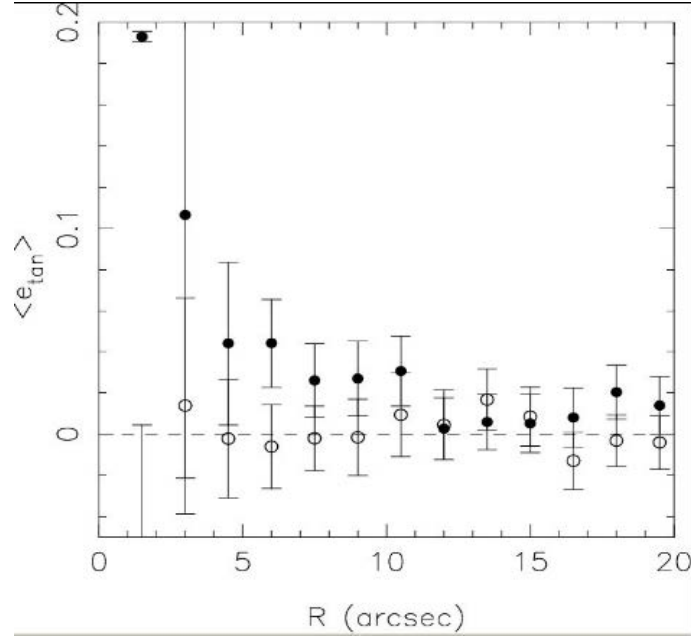


Figure 2.5: Weak Shear profile for the five stacked relaxed clusters. It should be noted that the innermost point at $R=1.5$ has anomalously small error bars due to a bug in the error plotting script and therefore should be disregarded.

profile. The result of subtracting this modified cluster signal from each of the five unrelaxed clusters was around a 5% change in some individual shear values in the stacked profile but nothing sufficiently significant to change the shape of the profile. The 15 arcsecond feature was largely unchanged and definitely still present. This left two possibilities, the first that the feature was some kind of residual so far unidentified in the subtraction of the cluster signal or possibly present in the original data catalogues, the second was that the effect had a physical origin. In discussions at Birmingham and at the LoCuSS group meeting in Chicago in early June 2008, several possibilities were presented by participants after this result had been shown. Some of the most promising were suggestions that the feature could be due to a characteristic clustering signal where this contribution to the shear profile was due to the average effect of all the cluster galaxies except the one involved in any specific pair distorting the source image in a coordinated way.

The findings of investigations made so far have led to several possibilities for continued study in the future. The origin of the profile features demonstrated in the weak shear profile of the stacked galaxy clusters has not yet been satisfactorily explained. The analysis in this section also did not take into account scaling relations for cluster galaxies of different mass. More massive cluster galaxies will induce greater shear at the same pair separation than less massive galaxies. Due to all pairs being averaged to obtain the plot presented in Figures 2.2 to 2.6, this effect should be fairly unimportant but it will be important to take into account in future work where cluster galaxy halo parameters are derived from shear measurements. With regards to the suggestion that the 15 arcsecond feature could be due to some coordinated clustering signal where the aggregate effect of all cluster galaxies on an image causes a characteristic profile feature on a certain scale, the next step towards testing if this is the case is to make a series of more complex shear maps for each of the clusters

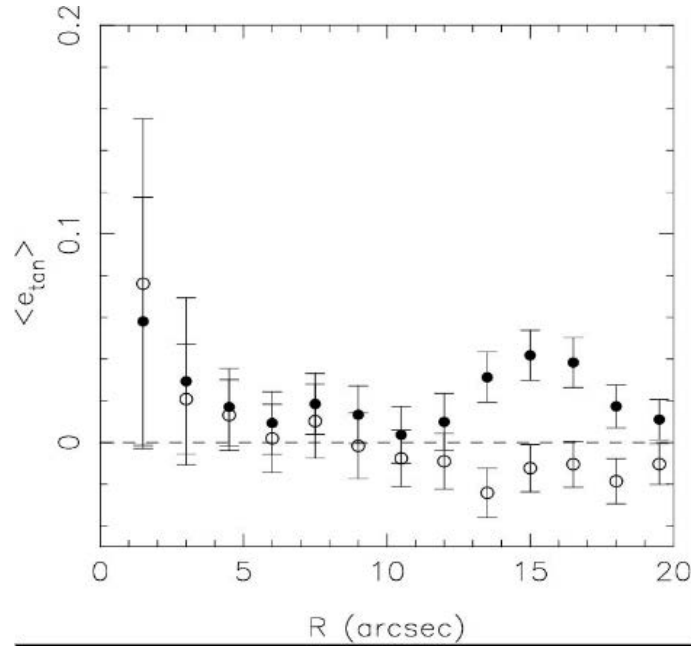


Figure 2.6: Weak Shear profile for the five stacked unrelaxed clusters.

in the sample. Each map would contain not only the relevant cluster potentials but also smaller potentials modelling the presence of all the cluster galaxies except the one involved in any given pair. Looping a script over say, 50 such maps per cluster should then give the shear signal only due to the cluster galaxy in the pair, omitting the contribution to the shear from other cluster galaxies. If the 15 arcsecond feature is due to a clustering signal, it is expected that it will be absent in any profile generated by a method so described. At this point, rather than study this 15 arcsecond anomaly in further detail, it was decided to study a dataset independent of this initial sample in order to see whether the same effect could be observed. If this is the case then a more detailed investigation can be performed on the nature of the anomaly.

Chapter 3

Galaxy-Galaxy Weak Lensing Simulations

3.1 Simulation Design

In order to expand the scope of the galaxy-galaxy weak lensing analysis beyond the ten clusters in the LoCuSS pilot survey, a larger sample of lensed faint galaxy catalogues was required. A sample of this nature, using the Subaru optical telescope to study thirty massive galaxy clusters has recently been completed by a LoCuSS collaborator [30]. An important part of the weak lensing analysis conducted on the previous sample of ten clusters was the removal in each case of the smooth cluster component contribution to the measured shear of the faint background galaxies. The assumption in Okabe et al. (2010) [23] was that each cluster component was simply a spherically symmetrical mass distribution. Subtraction of the smooth cluster potential from the data analysed from the previous sample was critical in extracting a measurable galaxy-galaxy weak lensing signal. A series of simulations was proposed in order to investigate the effect of subtracting inaccurate models of the cluster scale potential on a measured weak lensing signal. It was expected that the greater the deviation of the smooth cluster model from the reality, the more profound the effect on the measured signal. The magnitude of this deviation would then allow identification of the parameters that were most important to successfully describe the smooth cluster potential.

The simplifications made in Okabe 2010 were twofold. Each model assumed spherical symmetry which, based on the weak lensing mass maps in the same paper did not seem well justified as the majority of the clusters were generally elliptical. Secondly, the models only featured single halos for each cluster, when the mass maps suggested that many of the clusters in this sample could only be well described by multi-component models. The effects of both of these assumptions along with an under/overestimate of cluster potential mass were selected to be tested by simulation.

A schematic of the simulation procedure is shown in Figure 3.1.

For each test case, a catalogue of 40000 randomly positioned faint background galaxies at redshift 1 was produced in a 6.6Mpc x 6.6Mpc frame representative of a Subaru Suprimecam field. This data is referred to as the source catalogue in Figure 3.1. A model representing the 'true' cluster potential (which, during real observations would be unknown) was constructed with an NFW density profile [22] (Figure 3.1's 'truth' model) and was input into the Lenstool software. Running Lenstool then produced a catalogue of the sources after being lensed by the 'true' potential, the image catalogue. In order to simulate the effects of subtracting

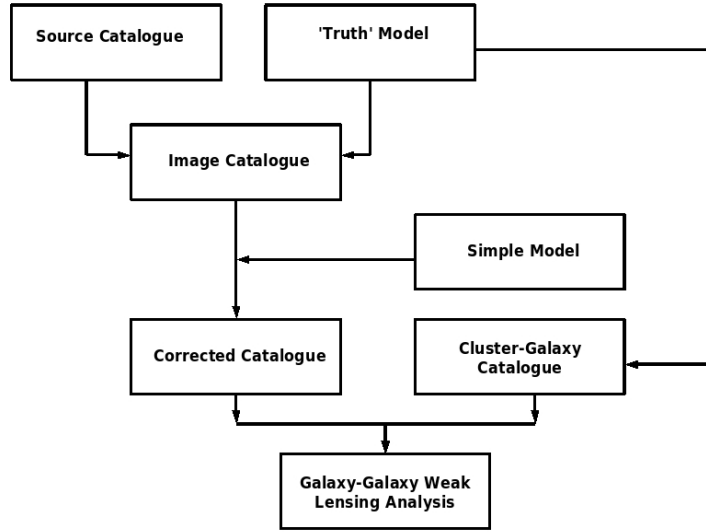


Figure 3.1: Schematic algorithm for Simulation design.

poorly parameterised models from the image catalogue, several simplified cluster potentials were also modelled using Lenstool. To measure the galaxy-galaxy shear signal, cluster galaxies must also be added to the simulation to allow foreground-background galaxy pairs to be formed (as in the previous chapter). They were approximated to truncated Pseudo-Isothermal Elliptical Mass Distributions (PIEMDs), described in Kassiola and Kovner 1993, at a redshift of 0.2 with a velocity dispersion of 180km/s and a cut radius of 30kpc. The shear caused by the simplified cluster potentials would be evaluated at the location of each faint background galaxy in the frame and subtracted from each by a vector sum resulting in Figure 3.1's corrected catalogue. In the ideal case where the simplified model is exactly equivalent to the 'truth' model, this should then leave only the shear signal due to the cluster galaxy perturbers. In the non-ideal case where the simplified and 'truth' models are different, it was hypothesised that some detectable residual shear signal from the poorly parameterised cluster subtraction will remain overlaid with the cluster galaxy shear signal, damaging our ability to extract a signal from the data (the Galaxy-galaxy weak lensing analysis in Figure 3.1). The cases to be tested in the simulation work had 'truth' models based on two cluster archetypes. The first a single halo elliptical mass distribution of $10^{15} M_{\odot}$, a concentration parameter (a measure of the density of matter within the cluster indicative of its formation epoch) value of 5 and an ellipticity of 0.3. A model with the same mass but circular (ie. Ellipticity 0) will be subtracted in order to assess the impact of selecting the wrong ellipticity in a cluster subtraction model. The second cluster archetype to be examined by this investigation is a two-component cluster potential. Many of the clusters examined in Okabe et al 2009 could not be well described by a single mass component and so more complex multi-component models of such clusters may be required in order to properly remove the shear contribution of the smooth cluster potential. The simulation will comprise two unequal mass components with one component 4 times the mass of the lesser. The masses chosen for the simulation are 8×10^{14} and 2×10^{14} solar masses respectively with a total halo mass equivalent to that examined for the single halo model. From this two-component simulation, will be removed models similar in nature to those described

for the single halo simulation with some distinctions due to the increased complexity of the simulation at hand. To investigate the effect of a poor parameterisation of the halo masses, a model will be subtracted from this simulation with a different mass ratio for the two components eg. Setting the mass of both components to be equal, at once causing an overestimate of the mass of the lesser component while also causing an underestimate of the mass of the greater. A further test unique to the two-component simulation is the effect of only modelling the larger of the two mass components. In this case, the larger mass component would be correctly parameterised in the subtraction model while the smaller mass component would be ignored. This test will simulate the assumption of a single-halo mass model for clusters poorly described by such a model.

By generating the perturber-centric shear profile for the cases described above, a picture of the effect of poorly parameterised cluster mass model subtraction will be built up and those assumptions which cause the largest deviation in the observed shearfield may be identified. By inspection of these results, the question of the importance of proper cluster modelling in the detection of galaxy-galaxy weak lensing may be addressed.

3.2 Preliminary Simulation Results

The simulations mentioned in previous sections to determine the effects of poor parameterisation of cluster modelling on the perturber-centric shear profile have been carried out for the case of incorrect cluster ellipticity. The results presented here comprise the model tests for the single-halo simulation as previously described.

The plot presented in figure 3.2 shows the average perturber induced shear field with no cluster subtraction having taken place. It is worth noting that even on a logarithmic scale, a relatively high degree of noise is induced in the profile even in regions outside the centre of the cluster (note the green line) by the effect of the cluster upon the background galaxy shapes. This is exactly the type of distortion of the shear profile that a well parameterised subtraction of the cluster signal aims to reduce. The central region within 0.5Mpc of the cluster centre (cyan line) where the influence of the smooth potential is greatest shows a large deviation from the ideal profile with some values going to negative tangential shear. Compare the result shown in this plot to the shear profile presented in figure 3.3 which shows the shear contribution from the perturbing cluster galaxy potentials only. Here, the profile is less noisy and follows a truncated PIEMD profile. It is this 'pure' signal that is the ultimate goal of the subtraction of the cluster signal and as such, the profile due to subtraction of any model from the single-halo simulation should be compared to that presented in figure 3.3. The scatter around the idealised profile demonstrated in the innermost cyan profile is due to the small number of possible cluster galaxy-faint galaxy pairings possible in this small region of the frame (several hundred compared to more than 10^4 in the region at radius greater than 1.5Mpc), it is expected that a larger number of faint background galaxies would alleviate this. It is worth mentioning at this stage that the differences in the shear profiles for these plots are relatively small on the larger scales (specifically the red and green profiles) due to the large size of each field. The Suprime-cam scale 34'x27' field allows the observer to probe out to several times the virial radius of the cluster around 3Mpc whereas the WFPC2 images that were used for the pilot study 10 cluster analysis were only large enough to examine the cluster core at less than 1Mpc. The effect of such large fields is to place a large proportion of the perturber-background galaxy pairs outside the distorting influence of the smooth cluster potential at that frame's centre. When such a large number of pairs is then averaged to produce the shearfield, those faint galaxies which are strongly influenced by the cluster potential have their effect on the shearfield attenuated by the sheer weight of numbers of

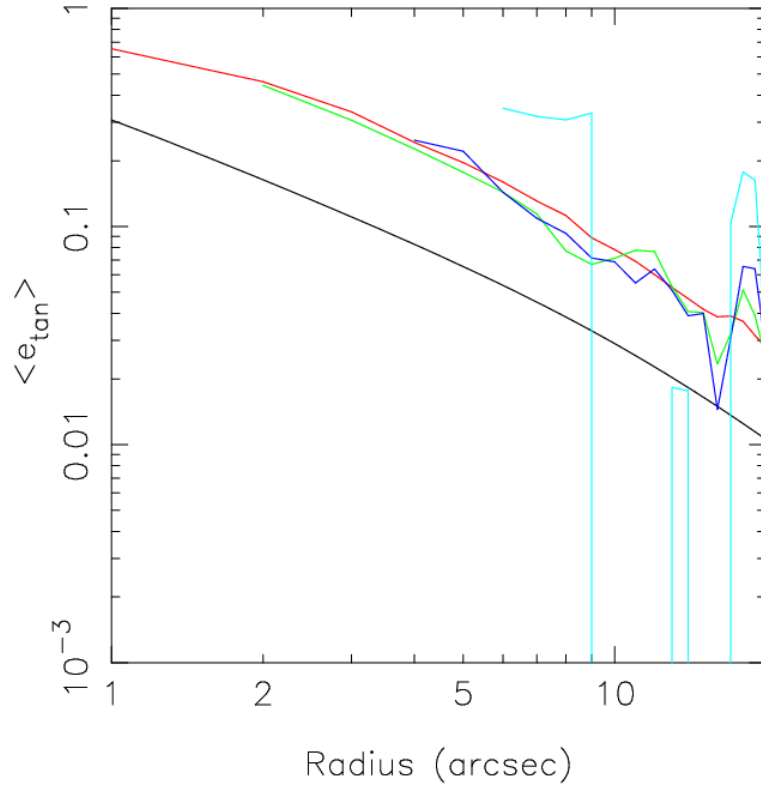


Figure 3.2: The Perturber-centric shear profile on a log-log scale for the simulated cluster with no cluster subtraction. The black solid line (offset by 0.2 on the y-axis for clarity) represents the logarithmic profile slope due to the effect of a truncated pseudo-isothermal elliptical mass distribution for comparison to the simulation shear profiles represented by the coloured lines with red showing the shear profile for faint lensed galaxy images outside 1.5Mpc from the cluster centre, green showing the profile for images between 1.5 and 1Mpc, dark blue showing the profile for images between 1Mpc and 0.5Mpc and finally cyan showing the profile for images less than 0.5Mpc from the cluster centre.

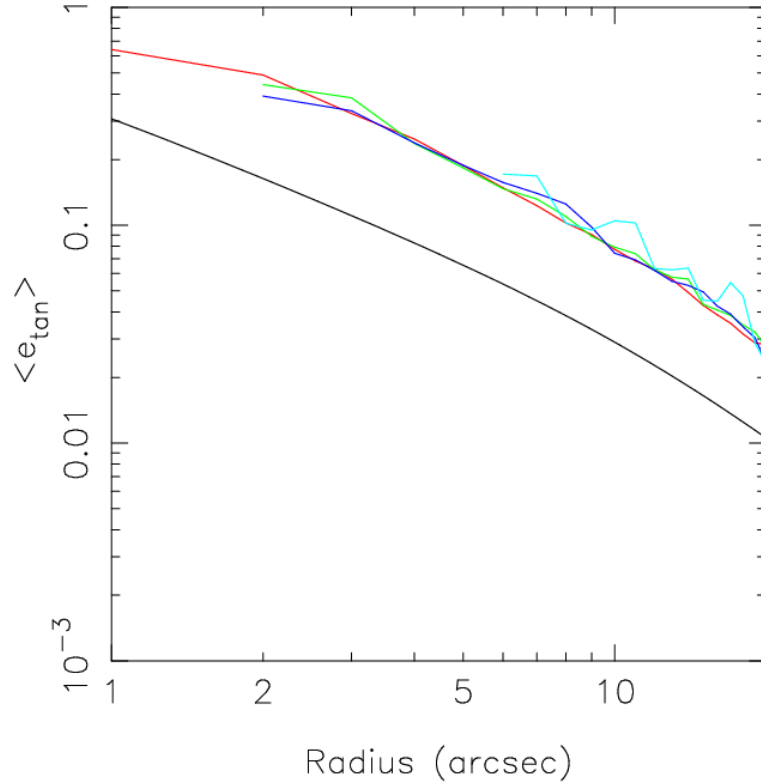


Figure 3.3: The Perturber-centric shear profile on a log-log scale due solely to the perturber signal. For plot key see Fig. 3.2 caption.

those pairs where the effects of the cluster potential is very weak. What this may show even in the early phase of the simulation work is that for larger fields, such as those examined by Subaru Suprime-cam, the effect of the cluster potential on the observed shear signal is not as great as it would be for a smaller frame such as that of the WFPC2 instrument. It then follows that the importance of a good parameterisation for such a smooth potential for the purposes of subtraction from an image catalogue will be proportionally less the larger (in solid angle) the frame under consideration.

The result of a test of the subtraction procedures used for this work can be seen in the plot figure 3.4. Here, the model that has been subtracted from the simulated cluster has the exact same parameters as those of the original simulated cluster. The result is very similar in appearance to that of the pure signal shown in figure 3.3 and much of the noise present in the unsubtracted profile of figure 3.2 has been removed, especially in the core regions of the cluster. With this test completed, the next step was to try the subtraction of a model which differed from the original simulation, the simplest of which was a simple change of the ellipticity of the smooth component from 0.3 to 0.0. The results of such a subtraction are shown in figure 3.5 where as can be seen, the profile once again demonstrates some of the noise seen in the non subtracted plot in figure 3.2 (although somewhat less drastically). This seems to show that although the result of a poor choice of a value such as ellipticity is subtle until scales of under 1Mpc are reached, at this point a deviation of around 0.02 in the shear signal may be observed for pairs separated by more than 10 arcseconds. The deviation on the

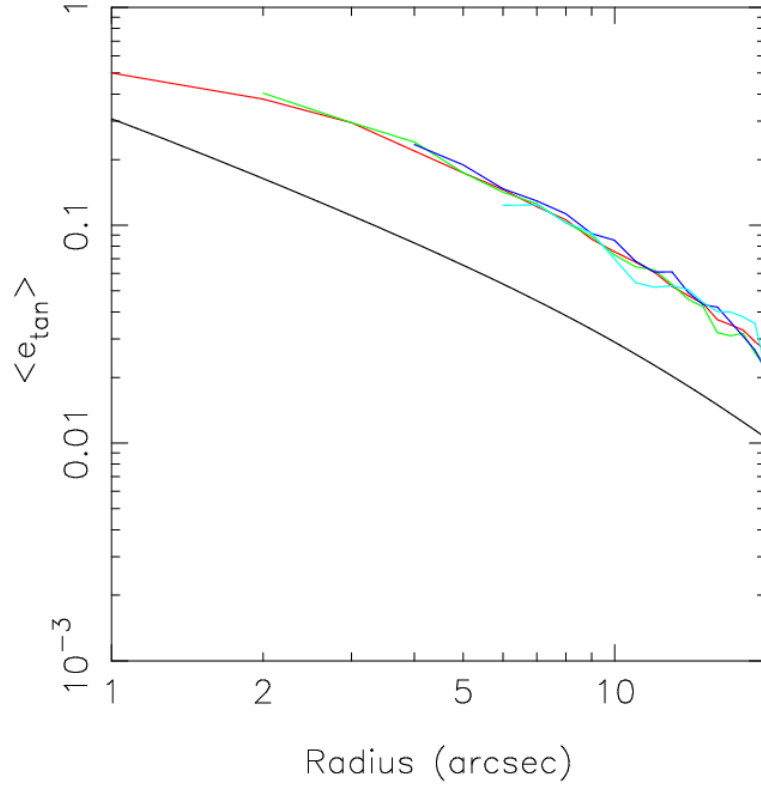


Figure 3.4: The Perturber-centric shear profile on a log-log scale for the simulated cluster with a model exactly matching the original smooth cluster parameters For plot key see Fig. 3.2 caption.

plot of figure 3.2 seems to be significant (cf. Figure 2.2 whose value at around 15 arcseconds separation is of the same order as the fluctuations in Figure 3.2). However, it must be noted that the number of foreground-background pairs contained within each clustercentric interval (i.e. Each line on the plot) is significantly reduced compared with the total number of pairs in the frame. From a total sample of 40000 faint background galaxies, only around 5000 are contained within 1Mpc (represented by the dark blue line on Figures 3.2-3.5) meaning that by the error formula presented in Chapter 2, (where the error scales with $1/\sqrt{n}$) the amplitude of the error on each bin has increased by a factor of ~ 3 . Comparing this to the error values in Figure 2.2 gives an error bar comparable to the magnitude of the result (with an amplitude of around 0.03 compared with Figure 2.2 which has an error amplitude closer to 0.01) so it is not possible to call the fluctuations statistically significant. It is predicted that after a similar treatment is carried out for the two-component simulation, the effects of the subtraction of models with incorrect clump mass ratios, or indeed those models which entirely neglect to model one of the mass components will be greater than those already observed for an incorrect assumption of the value of the cluster ellipticity. Although the effects thus-far observed are small on anything but the smallest cluster scales, they introduce fluctuations into the shear profile which will become more apparent at greater significance with refinements to the simulation process discussed in the next section.

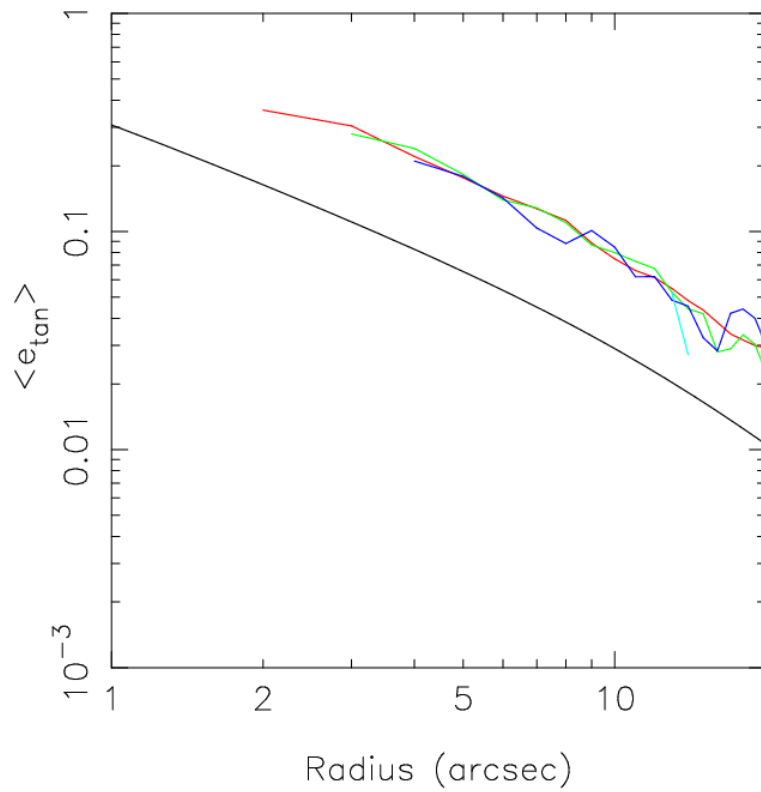


Figure 3.5: The Perturber-centric shear profile on a log-log scale for the simulated elliptical cluster with a model of the same mass but zero ellipticity. For plot key see Fig. 3.2 caption.

3.3 Simulation Refinement

In order to more generally test the effects of improper cluster scale shear signal subtraction, several changes and refinements to the simulated shear catalogues were required. It was decided that in order to measure the residual cluster shear signal most accurately, a different approach to shear modelling could be used. Rather than sampling the shear signal in annular bins for the whole cluster, considerably smaller but much higher resolution 'subgrids' could be designed and then placed in cluster environments of interest. Using LENSTOOL, a box of side length 20 arcseconds was chosen giving an exceptionally high sample density (considerably higher than would be expected from using the faint galaxies from even the deepest Hubble images). Each point in this 200x200 shearfield was then assigned an ellipticity by randomly sampling values from a faint galaxy ellipticity distribution derived from the Subaru SuprimeCam faint galaxy data from Okabe et al 2010 [23]. It was important to assign the individual points in the shearfield ellipticities as this approach would ascertain whether the effect of any residual cluster-scale shear signal was measurable above the intrinsic noise of a random ellipticity distribution. The Subaru weak lensing survey was chosen as a source of ellipticity information due to its scale and richness of data. By assigning ellipticities derived from an observed ellipticity distribution, it was hoped that measurements on the simulation would mirror measurements on a real dataset as closely as possible.

Each of the environments chosen for examination in the cluster was the centre of one of the 200x200 shearfields. In contrast to the previous simulations where the centre point would be occupied with a simulated cluster galaxy, this was no longer the case. Since shear values may be added linearly, measuring the cluster shear signal without the addition of a galaxy-scale perturber is a valid way to measure any cluster-scale shear signal at a given location and so cluster galaxies were not modelled in these new simulations.

The scenario to be most closely examined in this phase of simulation was the case where the true cluster mass profile was most closely approximated by a two halo model while that assigned to it by the observer (the simple model) was only a single halo mass model. Work using the previous simulation regime detailed in the previous section had shown only a very slight deviation in the measured shear signal when an incorrect ellipticity had been chosen for the cluster model and it was predicted that if a residual cluster signal was to be measurable, it would be in the scenario where the number of cluster mass components in the test model was incorrect. The cluster model chosen for this stage of the investigation was a double-halo potential with unequal mass components.

In order to compare the measured residual signals to a 'control' signal, a second set of 200x200 point shearfields were generated by Lenstool with no cluster component present essentially allowing the shear calculation to be carried out upon a physically accurate (and nominally 'uninteresting') area of faint background galaxies with no intervening cluster potential.

The difference between this approach and the full cluster averaged simulation results presented previously was the choice of cluster environments for examination. The previous approach involved averaging the galaxy-galaxy weak lensing signal over all perturbers in a cluster frame, stacked to obtain the highest possible signal to noise ratio. In this refinement, the analysis would be limited to specific, pre-determined environments in the cluster frame. The nature of the galaxy-galaxy weak lensing signals means that several different catalogues of faint galaxies will need to be generated, effectively creating several cluster frames whose regions can then be stacked in order to obtain a sufficient signal to noise ratio. The regions chosen for examination were selected to provide an environmentally varied dataset to draw conclusions from. The environments of interest were defined as shown in Fig 3.6 the centre-point between the two cluster scale mass components (which were aligned along the X-axis)

in an area defined as the 'saddle' region of the cluster, behind both mass components at a distance of 200 arcseconds from the cluster centre and another set of points at distances of 400 and 600 arcseconds. Other regions were selected off the X-axis above both cluster mass components at distances of 400 arcseconds and, in order to examine the possible residual signal in the outer region of the cluster, two points were chosen at coordinates of (900,900) and (-900,-900)

In order to assess the relative importance of the residual cluster signal, it was decided to superimpose upon each result the idealised shear signal from an L^* cluster galaxy allowing it to be easily determined whether the magnitude of the residual signal was great enough to be comparable to the desired galaxy-galaxy weak lensing signal. It was assumed that if the residual signal was of the same order of magnitude as the perturber scale signal of an L^* galaxy that complex cluster modelling and subtraction would be necessary in order to feasibly retrieve a weak lensing signal.

Considering the high sampling density of the generated shearfields, fewer cluster frames would be required to be stacked in order to obtain a sufficient signal to noise ratio for a feasible signal to be measured. However, in order to bring the number of samples examined in line with the theorised number from a Subaru SuprimeCam frame, it was decided that 4 frames should be stacked.

The results of this analysis were conclusive and the result became apparent even before the full selection of regions had been examined. In the interests of brevity, many of the plots of the shear signal regions have been omitted from this report and only a sample of figures have been included. It was hypothesised before the study was carried out that it would be the saddle region of the multi-halo cluster that would exhibit the largest residual signal from improper cluster subtraction and Figure 3.7 shows the extent of this signal. The figure contains a reference curve in black that represents the theoretical ideal shear signal from an L^* cluster galaxy at a redshift of 0.2, the average redshift of the clusters in the Subaru SuprimeCam sample. This reference line also includes error bars that represent the magnitude of the errors in shear measurement expected given the number density of galaxies on a Subaru frame. These error bars increase in size with decreasing pair separation as the annulus closest to the perturber is smaller and therefore will contain fewer faint galaxies (a typical Subaru observation contains around 20 background galaxies per square arcminute). The error bars decrease in magnitude at larger pair separations due to the increased number of faint galaxies in the much larger sampling annuli at larger pair separations. The green curve represents the 'control' signal and is purely derived from measuring the shear signal at the region centre using a faint galaxy catalogue with no potential to distort the image shapes. As can be seen, this curve is not perfectly flat showing that even with no perturbation at all, the measured shear signal is non-zero although it exhibits no correlation with pair separation, as expected.

The presented results are essentially a full cross-section of the differing plots obtained. Figure 3.7 details the shear signal derived from the region centred within the saddle region of the multi-halo cluster. Perhaps counter-intuitively, for the lowest separation of region centre and faint galaxy sample exhibited no apparent shear signal (theoretically, one would expect the lowest separation to exhibit the strongest shear signal, cf. the theoretical black PIEMD shear curve) however, at centre-sample separations on 5 arcseconds, the measured residual shear signal represented by the red curve is clearly comparable to the theoretical perturber shear signal. This trend continues with the residual signal remaining comparable and in fact tending to the upper bounds of the theoretical ideal shear signal. Compare this result to Figure 3.8 which details the shear signal for the sample field centred 400 arcseconds from the frame centre along the X-axis (essentially behind the smaller of the two

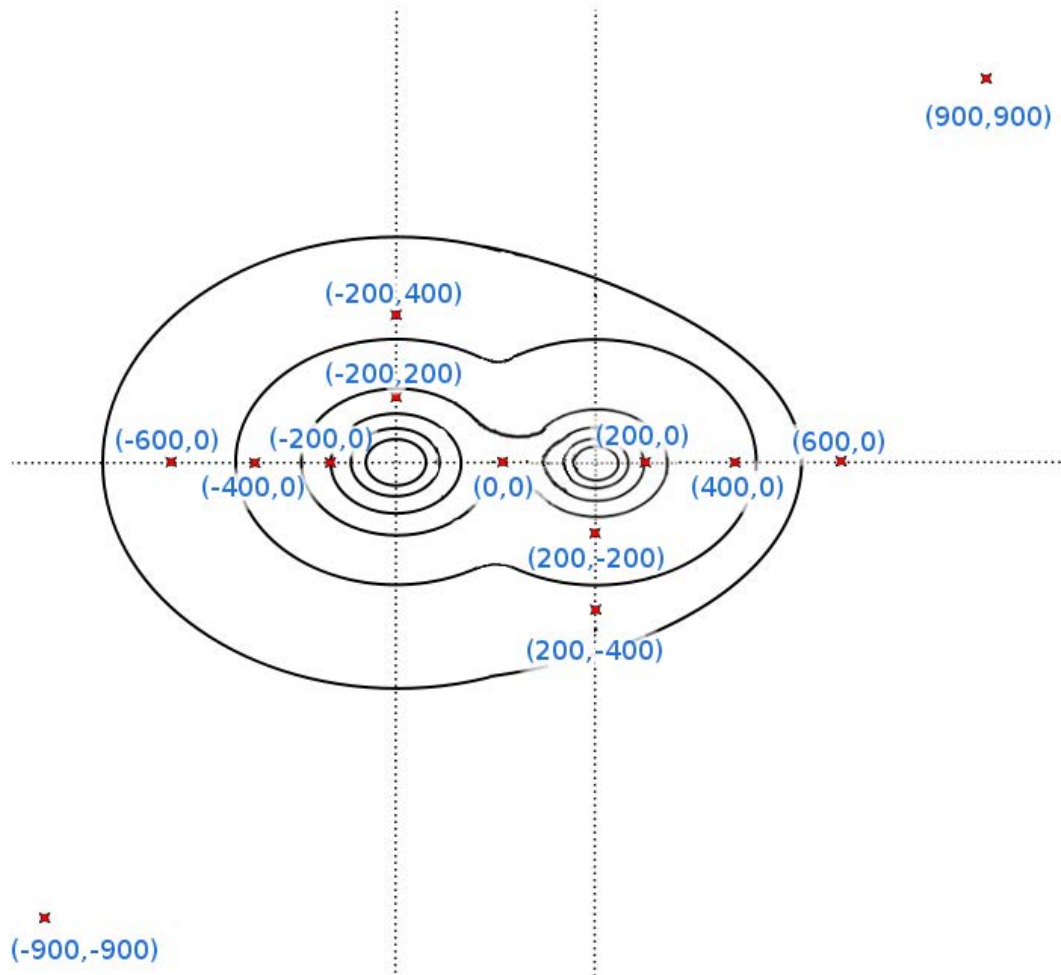


Figure 3.6: The schematic model of the bimodal simulation cluster. Potentials are described with contours with the most massive potential on the left. The points at which LENSSTOOL sampling was carried out are highlighted in red. Note the saddle region at $(0,0)$ where the magnitude of a residual cluster shear signal is suspected to be largest.

halo mass components) This region corresponds to approximately 1.2 Mpc from the cluster centre at a redshift of 0.2 and so probes the virial radius of the cluster. The red curve in this plot does not differ in any significant way from the green curve control signal, which represents the measured shear signal from the patch of simulated sky under consideration with no perturbers. Any differences between the two curves can be attributed to the different ellipticity values sampled to make the different catalogues.

The remainder of the regions sampled by this method all exhibited extremely similar behaviour to that shown in Figures 3.8, 3.9 and 3.10. There was no appreciable difference in the residual cluster shear signal whether the region sampled was 200 or 900 arcseconds from the cluster centre with the residual curve exhibiting only the very minor fluctuations due to the intrinsic ellipticity distribution. The saddle region was the only example of a detectable residual shear signal in the study.

The conclusion drawn from these results was quite contrary to the original prediction of the importance of accurate cluster modelling. In the relatively extreme case examined in this phase of the study, namely a mismatch in the number of halo mass components, we wished to measure the magnitude of this systematic effect to assess whether it was significant enough to have an impact on the weak shear measurement. That the only region that exhibited any signal was the saddle region was unexpected however it does allow an important conclusion to be reached; that the quality (or indeed presence) of cluster potential subtraction is inconsequential to the measurement of a galaxy-galaxy weak lensing signal in all but the saddle regions of multi-halo clusters. This means that the relatively simple cluster models exhibited in Okabe et al 2010 [23] are sufficiently sophisticated to allow measurement of the galaxy-galaxy weak lensing signal with no further work required to increase the complexity of the cluster models.

This allows the currently available Subaru SuprimeCam data to be used for galaxy-galaxy weak lensing detection without modification, an important conclusion as the quality of cluster subtraction was, until this point an untested unknown.

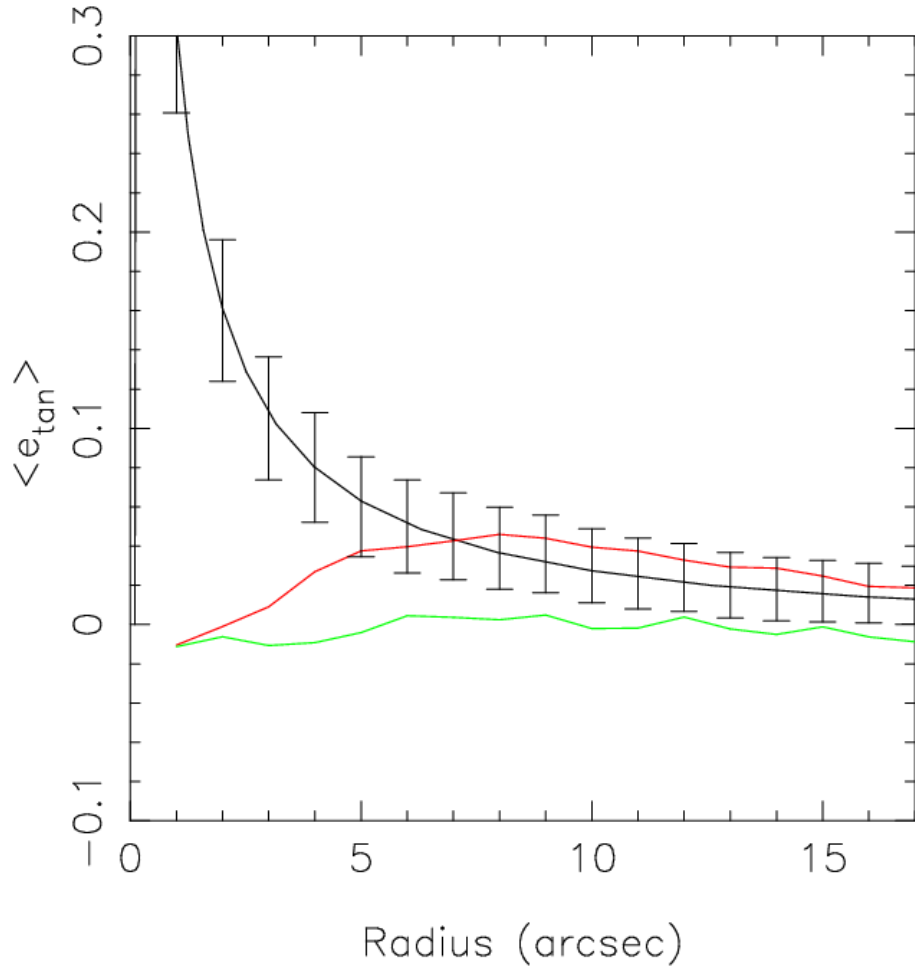


Figure 3.7: The stacked subgrid shear signal from the central saddle region of a 2-halo cluster model. The black curve represents the theoretical ideal shear signal from an L^* PIEMD cluster galaxy scale perturber. The red curve represents the measured shear signal from the unsubtracted saddle region. The green curve represents the shear signal due to the intrinsic scatter in ellipticity in background faint galaxies from a frame with no cluster-scale mass component.

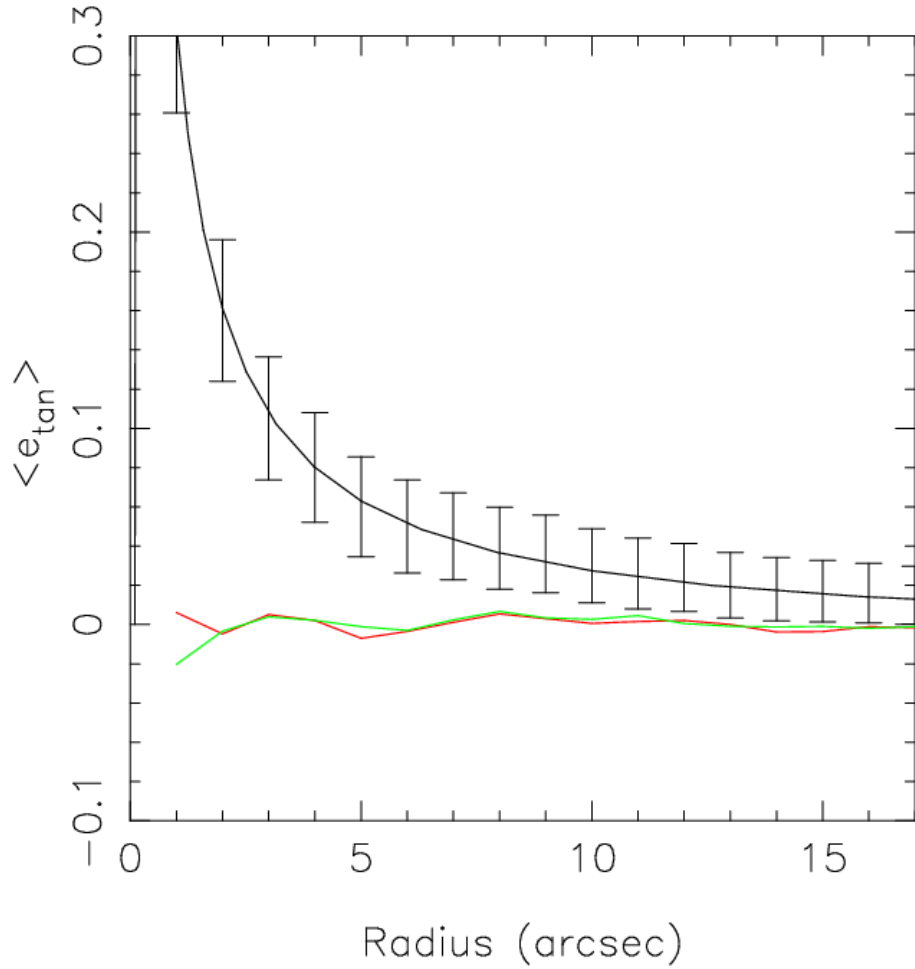


Figure 3.8: The stacked subgrid shear signal from a region displaced 400 arcseconds on the X-axis from the frame centre of a 2-halo cluster model. The black curve represents the theoretical ideal shear signal from an L^* PIEMD cluster galaxy scale perturber. The red curve represents the measured shear signal from the unsubtracted displaced region. The green curve represents the shear signal due to the intrinsic scatter in ellipticity in background faint galaxies from a frame with no cluster-scale mass component.

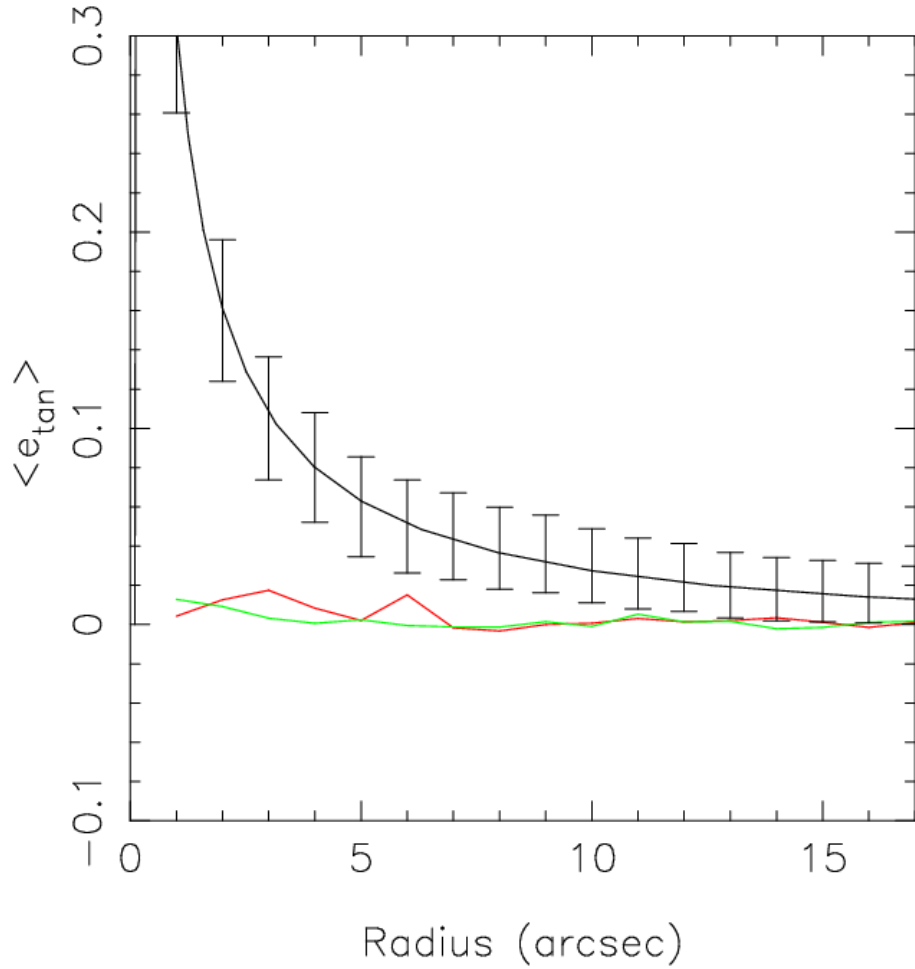


Figure 3.9: The stacked subgrid shear signal from a region displaced 200 arcseconds on the Y-axis from the frame centre of a 2-halo cluster model. The black curve represents the theoretical ideal shear signal from an L^* PIEMD cluster galaxy scale perturber. The red curve represents the measured shear signal from the unsubtracted displaced region. The green curve represents the shear signal due to the intrinsic scatter in ellipticity in background faint galaxies from a frame with no cluster-scale mass component.

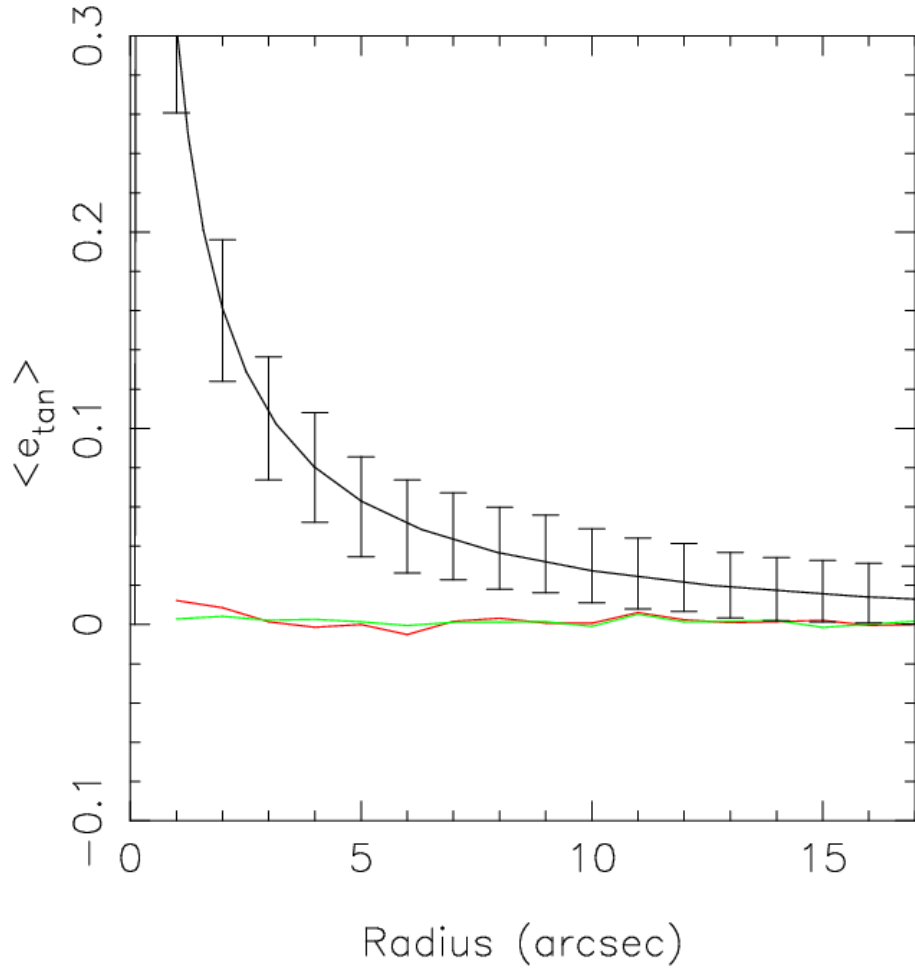


Figure 3.10: The stacked subgrid shear signal from a region displaced 400 arcseconds on the Y-axis from the frame centre of a 2-halo cluster model. The black curve represents the theoretical ideal shear signal from an L^* PIEMD cluster galaxy scale perturber. The red curve represents the measured shear signal from the unsubtracted displaced region. The green curve represents the shear signal due to the intrinsic scatter in ellipticity in background faint galaxies from a frame with no cluster-scale mass component.

Chapter 4

Mask Design

4.1 Cluster Observations

An important component of the work performed in this study has been the preparation for and undertaking of several observing runs designed to obtain new spectroscopic data for gravitationally lensed arcs in the core regions of massive galaxy clusters. The motivation for obtaining spectroscopic data for these objects is to determine the redshift of the arcs in each cluster. The use of redshift information in this investigation is twofold. Firstly, the redshift allows spectroscopic confirmation of multiple imaging in the cluster. If the spectra for the objects is found to put objects of similar morphology at the same redshift then the images are taken to be multiple images of the same lensed background object. With the redshift of an object confirmed, the second application of this information is the determination of the geometry of the source-lens system. Knowledge of this geometry and the mapping between images allows the mass distribution of the lensing cluster to be constrained and allows mapping of the cluster dark-matter halo. The redshift information therefore, provides the strong lensing constraints and a normalisation on the cluster mass model that enable an actual cluster mass to be derived. In order for the most complete and accurate model to be obtained, these constraints are used in concert with Weak lensing constraints from the outer regions of the cluster described earlier in this report.

4.2 Mask Design

In order to prepare for spectroscopic observations of objects within a cluster, a mask must be designed for the instrument to be used for observation in order that only light from the objects of interest on the telescope frame is dispersed into spectra. To accomplish this, a metal sheet of variable size dependent on the instrument under consideration is milled with slits which correspond to the positions (and to a limited extent, orientations) of the arcs and cluster galaxies that one wishes to observe. The preparation for this differs depending on the facility the mask is to be designed for although the fundamental aim in each case remains the same.

Accuracy at this stage is key to obtaining the results desired as the tolerances for astrometric error in an investigation of this nature are extremely low. The sources to be observed are typically of the order of half an arcsecond in width (with corresponding slit widths of one arcsecond) so relatively small errors in positioning of the slits could cause serious attenuation or total loss of the light from the desired source object. It is estimated that an

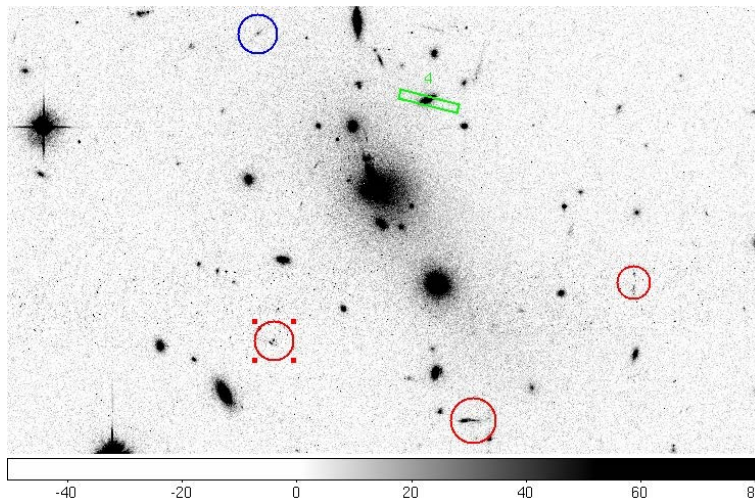


Figure 4.1: Detail taken from the core region of the RXCJ0307 HST frame. Multiple image candidates for observation are shown in red with the visible tangential counterimage circled in blue. A fifth radial image may also exist but is obscured by the BCG. Also shown in green is a cluster galaxy selected for observation on the RXCJ0307 mask.

error of 0.5 arcseconds on the VLT FORS instrument for example would result in a 60% attenuation of the source signal.

Gemini GMOS

The majority of mask design undertaken has been for the GMOS instrument at the Gemini South observatory in Chile. LoCuSS requested, and was awarded, 42 hours of observing time on GMOS in semester 2008A and 36 hours in 2008B running from February 2008 to January 2009. The requested targets were twelve galaxy clusters in the southern sky which had demonstrated interesting lensing features on HST imaging frames and so required spectroscopic follow-up for arc redshift determination.

Preimaging was taken using GMOS at the chosen position angles for each cluster for use in the design of the masks. Each preimage was the combination of five separate preimage frames with a total observation time per cluster preimage of 450 seconds. The mask design process involves selecting the objects of interest, defining slit parameters (width, length etc) and placing the slits in the mask. To accomplish this, Gemini provide software which allows the creation of an object definition file, a catalogue of the objects selected for spectroscopy and the parameters of the slit associated with that object. Within the object definition file, priorities for individual objects were set with gravitational arcs receiving the highest priority in the frame. The lower priorities were taken by cluster galaxies in order to make best use of the available space on the mask. The software would use a placing algorithm to generate the final mask given the desired parameters for each slit and would prioritise the placement of slits on lensed arcs.

A coordinate mapping process was required during mask design to confidently locate the target arcs. Determination of which clusters contained interesting arc candidates and accurate determination of the arc positions was obtained using Hubble Space Telescope image frames mostly taken with the ACS instrument although some were taken with the lower resolution WFPC2 instrument. Shallow exposure cluster preimages were then taken

using the same optical system that was to be used for the spectroscopic observations. In order to make use of the high resolution images from HST, the Hubble and preimage frames needed to have a commonly defined WCS solution so that the coordinate system of the HST frame matched that of the Gemini preimage frame (Gemini software requires slits be placed using X,Y image coordinates and not WCS coordinates). To do this, the HST frame was overlaid with a catalogue of known, relatively bright objects from the USNO B data repository that were visible in both the HST and Gemini preimage frames. The positions of these objects were tweaked in order to match the positions on the HST frame. The coordinates of these objects were output as a file then mapped onto the Gemini preimage frame where positions were again adjusted to match those of objects on the frame and then output similarly into a file. Using the differing coordinates in these two files, the IRAF routine GEOMAP was able to construct a linear transformation for mapping the coordinate system of the HST frame to that of the Gemini frame. A further IRAF routine, GEOTRAN, was then used to apply this WCS solution to the Hubble frame. This resulted in frames that were aligned to a precision greater than 0.5 arcseconds.

A sample of the core of the cluster RXCJ0237 in both Gemini preimaging quality (Figure 4.2) and the rectified HST quality (Figure 4.3) shows the comparative precision of the arc position in the HST frame, highlighting the need for the procedure described previously.

The interested reader is referred to the Appendix which contains images of each of the cluster cores selected for spectroscopic observations with GMOS. These images give an overall impression of the phenomena described previously with annotations for target objects of particular interest.

The cluster galaxies on the frame were selected by using SExtractor on the preimage frames which automatically identifies extended sources. A script was designed and run which then performed several cuts to the output catalogue from SExtractor, removing stars and imposing a magnitude cut at 22 in the R band. The remaining objects were then prioritised according to brightness with the brightest receiving higher priority for selection.

A total of 26 masks were produced for the GMOS observations, two masks for each cluster (except for RXCJ2308 which had 4 due to not being able to fit sufficient arcs from its complex image configuration onto a single mask). Each cluster was observed for two hours of integration time with four 15 minute exposures for each mask. The same top priority arc slits were chosen for both masks in each cluster pair with the masks differing in their choice of cluster galaxies only. This allowed the maximum two hour exposure for the faint gravitational arcs but only a single hour exposure for each of the cluster galaxies which did not require such deep spectroscopy.

An example completed mask design displayed in the GMOS software is displayed as Figure 4.4 with a zoomed in detail image of the core region arc positioning shown in Figure 4.5.

4.3 VLT FORS2

In addition to the GMOS observations, LoCuSS has also been awarded 2.6 nights of visitor mode observing time at the 8 metre VLT facility in Paranal, Chile. These observations which were carried out using the FORS2 instrument in late August and early September 2008 were motivated similarly to the GMOS observations, the determination of gravitationally lensed arc redshifts.

Similar to the GMOS observations, the mask design process involved rectification of existing HST frames to the coordinate system of the FORS2 preimaging. In this case, the proprietary mask design software provided by ESO required the slit coordinates to be entered

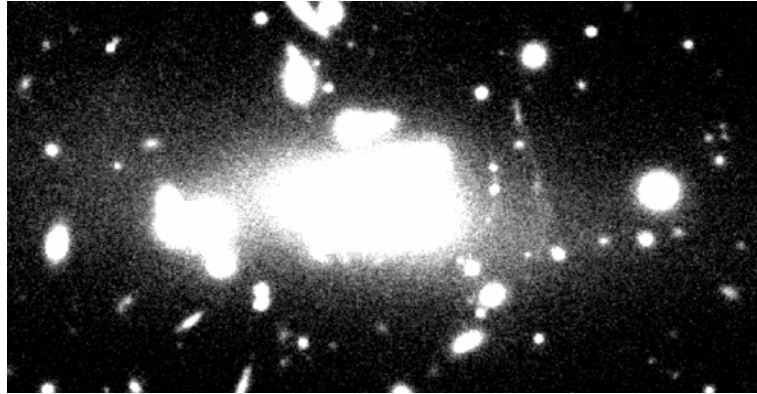


Figure 4.2: Sample of the core region of cluster RXCJ0237 taken from Gemini GMOS preimaging data

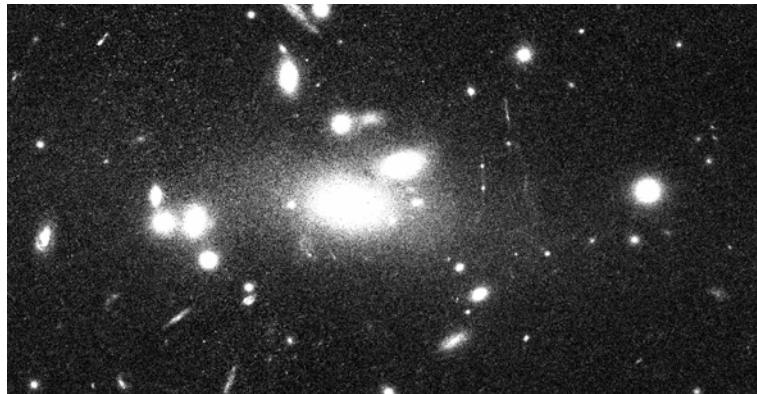


Figure 4.3: The same area of the core region of cluster RXCJ0237 taken from Hubble Space Telescope ACS data

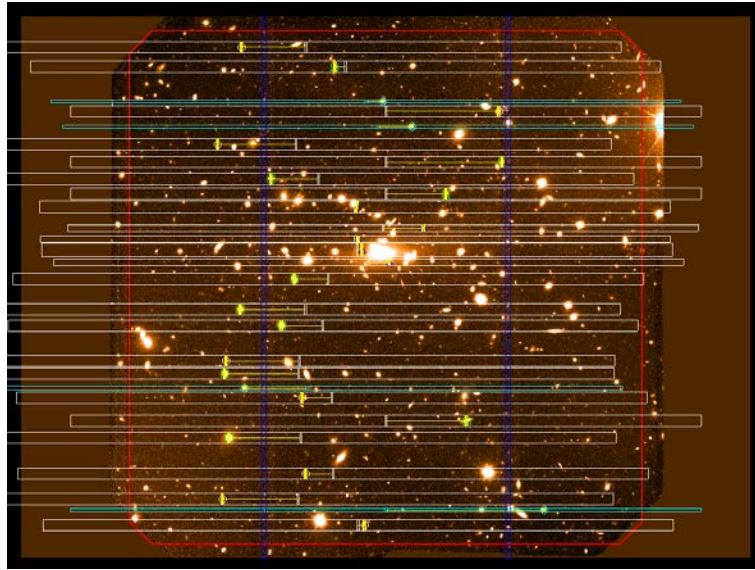


Figure 4.4: A finished Gemini GMOS mask design for the cluster RXCJ0237. The white rectangles show the dispersion axis for the individual object spectra. Vertical blue bars show the Gemini GMOS detector CCD chip gaps.

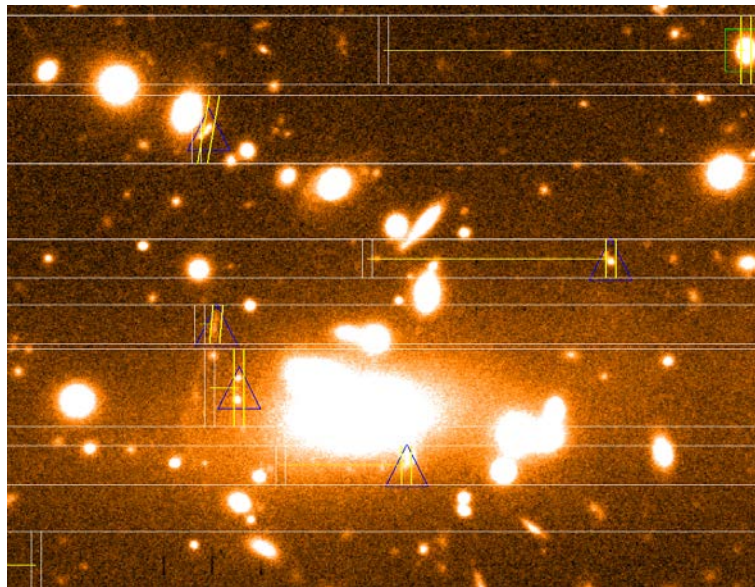


Figure 4.5: Detail of the same mask as the previous figure showing the core region of the cluster. Blue triangle markers represent those objects marked out for the highest priority observations, the gravitationally lensed images.

in terms of their right-ascension and declination rather than their image x,y coordinates. In order to do this, a different method was used to the previous rectification. The principle was similar, identification of the same sources in both images with differing coordinate systems with a routine to determine the transformation required to make that mapping work. The CCMAP and CCFIND routines within IRAF were invoked to make a FITS header adjustment to the HST frames, essentially replacing their WCS solution with that of the preimages which allowed precise identification of arc positions.

The FORS masks are similar to those for Gemini GMOS in that the slits took broadly the same form. Each slit was, by default, 1 arcsecond wide with a length of 10 arcseconds. Like the GMOS limitations, the FORS slits could be rotated up to 20 degrees off vertical in order to capture light from off-axis arcs which allowed some flexibility after the most efficient position angle for the frame had been selected.

While most of the clusters observed with the FORS instrument were unique to this observing run, there was some overlap with the cluster selection for the GMOS observing run. This allowed further confirmation of the spectroscopic redshifts for arcs that were observed with both instruments although an effort was made to examine different arcs with the different instruments where the full range of objects of interest could not be covered by a single instrument.

Chapter 5

Conclusions

The first aim of this investigation was to assess the feasibility of detecting a measurable galaxy-galaxy lensing shear signal in the core regions of massive clusters. In order to carry this out, it was found to be necessary to stack the cluster-galaxy scale shear signal of multiple galaxy clusters. As anticipated, the larger the number of galaxy pairs available for stacking, the better the signal to noise ratio of the resulting shear signal. It was shown that a signal was retrievable from a subset of the 10 X-ray selected clusters (splitting the sample into two still resulted in a measurable signal). An anomalous feature in the stacked galaxy-galaxy signal was observed in the subset of clusters which were unrelaxed, having recently participated in a major merger which was not present in the subset of clusters with relaxed morphologies. At present, the source of this anomaly is not well understood and nothing resembling this phenomenon was detected in the simulated cluster study conducted in later phases of this investigation. It is therefore of potential future interest for an independent study utilising a different dataset derived from these same clusters to be performed in order to assess whether this effect is indeed present universally or is an artifact of some bias in the dataset chosen for this work. Identification of such a coherent feature in multiple datasets could reveal as-yet unknown effects of cluster mergers upon individual cluster galaxies.

The work presented in this report has also endeavoured to investigate the magnitude of the systematic error in shear measurement due to improper, or indeed absent, cluster-scale potential subtraction. This study is the first known to have examined this as-yet overlooked systematic effect and has concluded that high precision in removing the shear effects of cluster-scale dark matter halos is unnecessary in almost all cases. The single case in which the systematic effect was found to be of the same order of magnitude as the galaxy-galaxy shear signal was a sampled area that lay in the saddle region of a massive, bimodal cluster. Although this result does show that the systematic can have an effect on the galaxy-galaxy signal, the relatively extreme location of this probe of the systematic would be a rare thing to sample with high frequency in any investigation using real observational data. This rarity, combined with the tendency of weak lensing investigations to omit the very central regions of a cluster for background galaxy selection (as in these regions, the linear regime of weak lensing breaks down and the non linear effects of strong lensing become dominant) mean that the systematic effect is of no concern for future galaxy-galaxy weak lensing studies. The later figures in section 3.3 demonstrate that the magnitude of the systematic for environments outside the cluster saddle region does not even approach the same order of magnitude as the idealised signal expected for a simulated cluster-galaxy scale PIEMD, a result that will hold true for any study with sufficient number density to detect a galaxy-galaxy signal. This conclusion should be of significant interest to studies attempting to use galaxy-galaxy weak

lensing to constrain the parameters of galaxy-scale dark matter halos as such studies need not expend time and effort modelling the smooth, cluster-scale dark matter halo with a high degree of accuracy.

The design of spectroscopic instrument masks is a key step in obtaining the strong lensing redshift constraints required for a determination of cluster mass through the normalisation of the cluster mass distribution. This study identified multiple arcs of interest in a sample of 14 massive galaxy clusters chosen for observation with the Gemini GMOS and VLT FORS instruments. Amongst the sample were several galaxy-galaxy strong lensing candidates which are potentially of great use in determining the mass profiles of cluster-galaxy scale dark matter halos without the statistical difficulties associated with the retrieval of a stacked galaxy-galaxy weak lensing signal. The comparative rarity of such phenomena however make such cases non-general enough to still require galaxy-galaxy weak lensing studies to determine the characteristics of the majority of cluster-galaxy scale dark matter halos. With the data taken from these observation runs, it is hoped that a more complete model of massive galaxy clusters will be able to be reconstructed with the union of weak, strong and galaxy-galaxy lensing techniques. Such accurate models of galaxy clusters will allow not only insights into the nature and evolution of the clusters around redshift 0.2 but will also have important impacts on the use of galaxy clusters as a cosmological probe, bettering our understanding of cosmology in general.

Chapter 6

Appendix: Cluster Strong-Lensing Observation Images

This appendix section gives an overview of the cluster cores selected for spectroscopic observations with the Gemini GMOS instrument. The intention is to give the reader annotated images of each of the clusters selected for observation with multiple image candidates highlighted to give a visual impression of these striking astronomical phenomena. Also included in some of these images are a number of strong galaxy-galaxy lensing candidates that were selected as objects of interest in this study. These are the strongly lensed analogue of the galaxy-galaxy weak lensing phenomena of key interest in this work and the ability to see the tangential distortions by simple visual inspection in these examples is good for illustrating an exaggerated instance of an otherwise obscure concept.

The targetting of the slits in these masks in some cases appears to miss portions of the arc under consideration. This is due to the need to include some portion of dark sky in each slit for accurate local sky subtraction during the data reduction phase. This allows the spectra to be cleaned more accurately and so increases the quality of the final spectroscopic data. In all cases however, every effort was made to ensure that the brightest portion of the arc was covered.

All images are taken with the high resolution ACS instrument on the Hubble Space telescope which provides an after-drizzle image resolution of 0.049 arcseconds per pixel, ideal for visually identifying arcs of interest. The images are presented aligned to WCS coordinates using the convention of North pointing upwards and East pointing to the left.

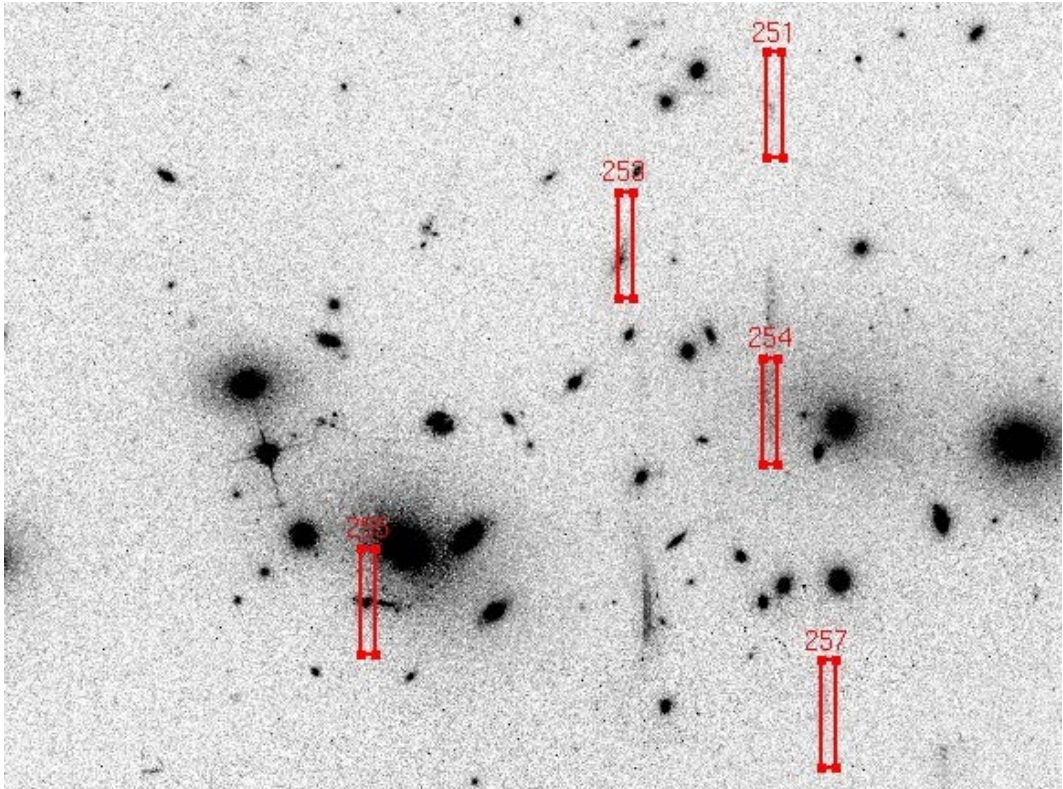


Figure 6.1: HST image showing the core region of the cluster RXCJ0043 with several strong-lensing arc candidates from the very bright Slit 255 arc near the BCG to fainter candidates as shown at slit 254. Note that the arc 254 South of the BCG appears to be one of a merging pair of images with the other image located to the right.

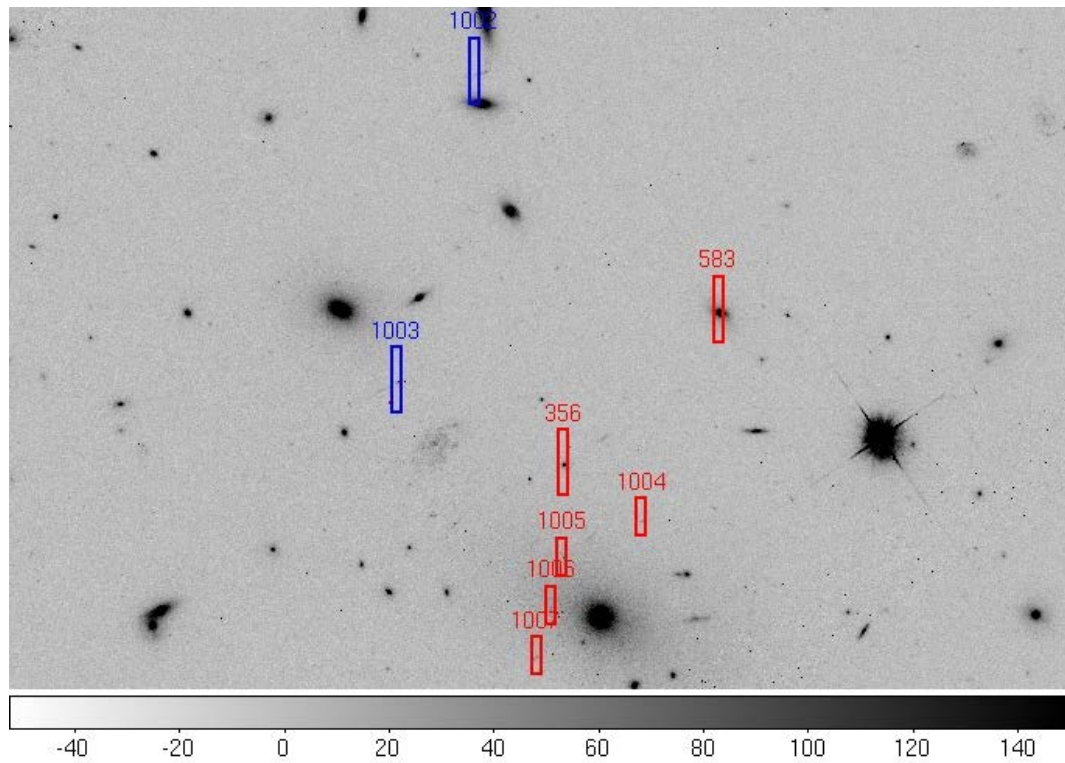


Figure 6.2: HST image showing the core region of RXCJ0118. Four possible multiple images are located near to the BCG, located at the left of the image, at slits 1004, 1005 1006 and 1007 it is expected that a much fainter radial counterimage exists under the flux from the BCG. Other possible arcs of interest are highlighted in blue (Slits 1002 and 1003) with potential galaxy-galaxy image distortion at slit 1002. Also pictured here (Slits 356 and 583) are typical cluster galaxies targeted for observation.

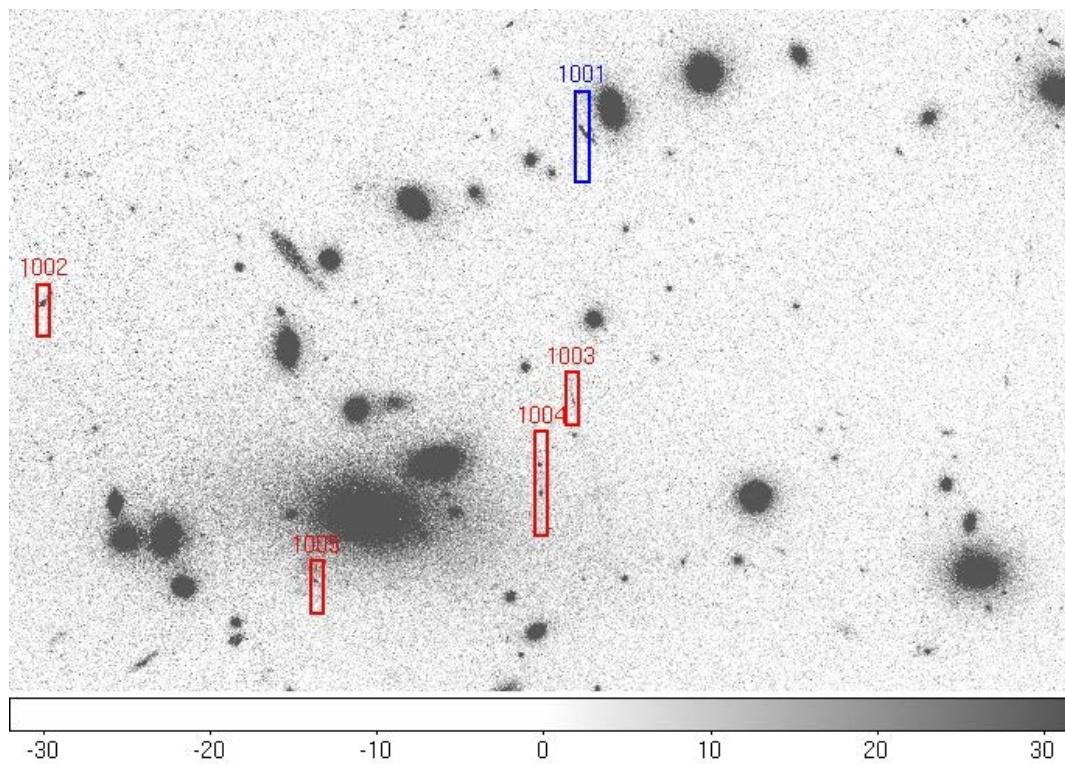


Figure 6.3: Image from the core region of the cluster RXCJ0237 featuring multiple image candidates in red including a merging image pair at slit 1004. A prominent galaxy-galaxy strong lens candidate can be seen in the North West of the image highlighted in blue. The BCG is located in the South East of the image.

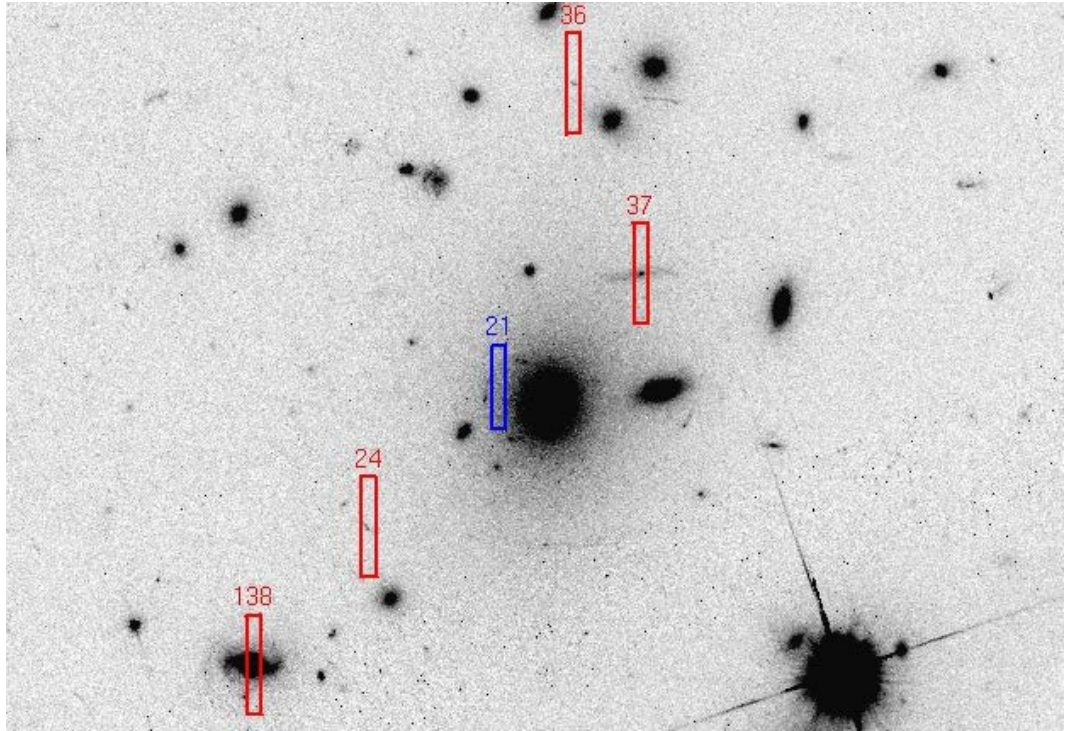


Figure 6.4: Image of the core region of the cluster RXCJ0304. This cluster features a highly interesting multiple image configuration. Slit 21 in blue targets the main arc feature in this cluster which is actually a merged arc of up to four images (a faint counterimage candidate can just be seen to the south of the BCG but was not selected for observation in this study). This configuration may be a physical manifestation of a hyperbolic umbilic catastrophe caustic arrangement, of which no observed example yet exists. Further studies will be required to ascertain if this is the case.

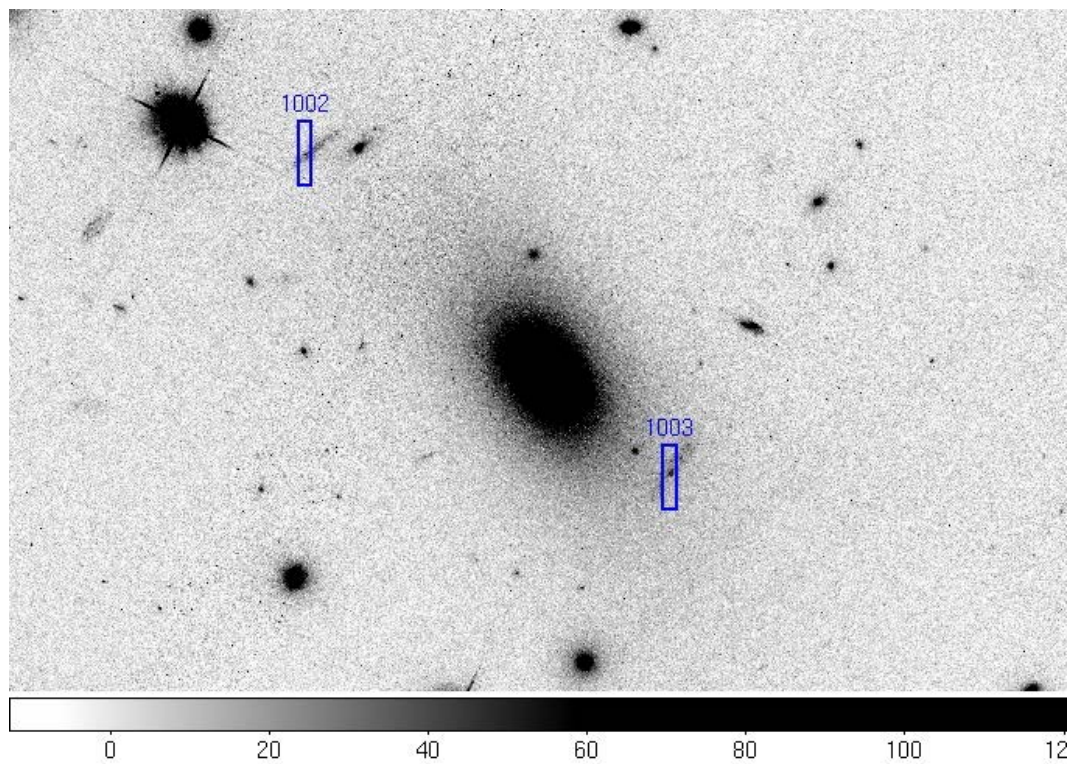


Figure 6.5: Image of the core region of the cluster RXCJ0527 with two strongly lensed candidates in blue. Despite the small number of arcs for observation in this cluster, their brightness is relatively high and the arcs quite isolated making for potentially strong and clean spectra.

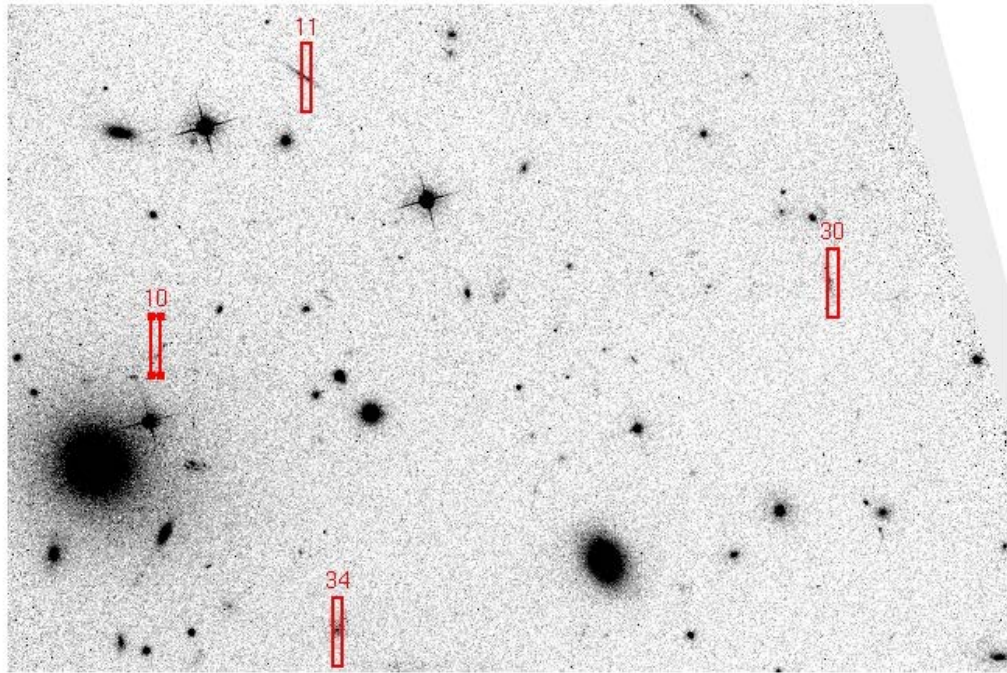


Figure 6.6: An image of the core region of RXCJ0547. This cluster had potential strong-lensing candidates located significantly further from the BCG (which is located in the mid-upper left) than in most of the other clusters in this sample. These arcs could be chance alignments of foreground or cluster redshift objects but spectroscopic redshifts are required to confirm this. Also of note is the object in slit 10 which may be a radially aligned arc. These radial arcs are often highly demagnified and located beneath the flux of the BCG so to find such an arc relatively far out from the BCG would be a highly interesting result.

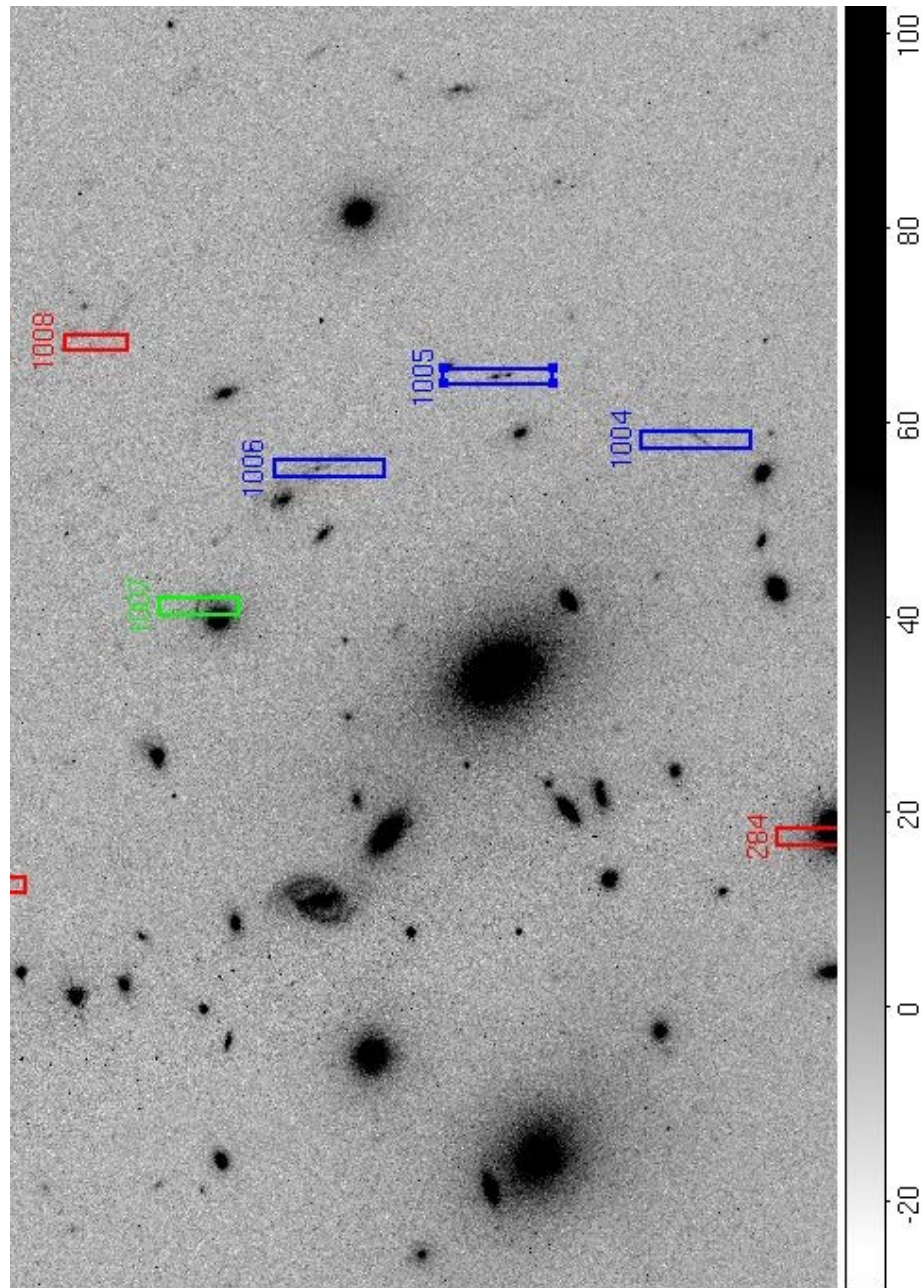


Figure 6.7: Image of the core region of RXCJ0638, an apparently arc-rich cluster with multiple areas of interest. Possible multiple images are highlighted in blue with a merging pair of images located at slit 1005. A fainter tangential arc can be seen in the North West of the image highlighted in red. Of particular interest is the object highlighted in green which is a highly prominent galaxy-galaxy strong lens candidate.

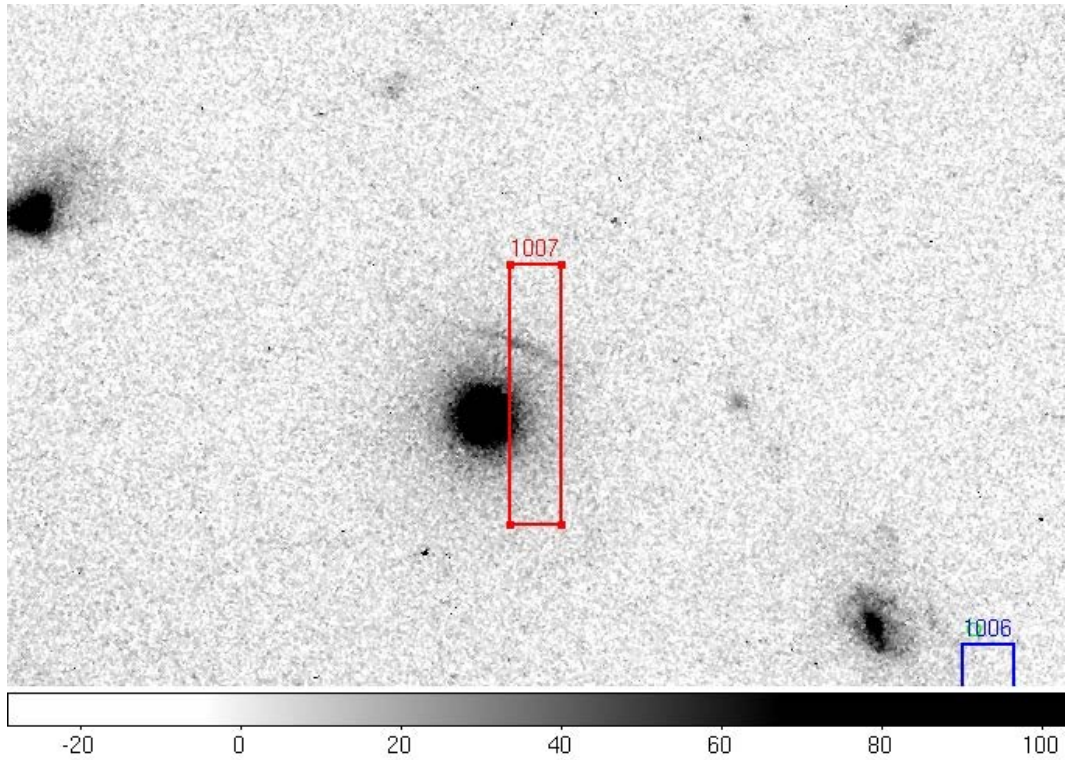


Figure 6.8: Closeup of the galaxy-galaxy strong lensing candidate identified in the RXCJ0638 frame. One of the most promising examples of cluster galaxy scale strong lensing in this sample. The faint, highly elongated nature of the arc suggests strongly that this is a faint background galaxy undergoing lensing magnification rather than a satellite feature of the cluster galaxy located to the south. The difficulty in reducing this type of spectrum is removing the overspill flux from the cluster galaxy which, at such small separations, can strongly influence the arc spectrum.

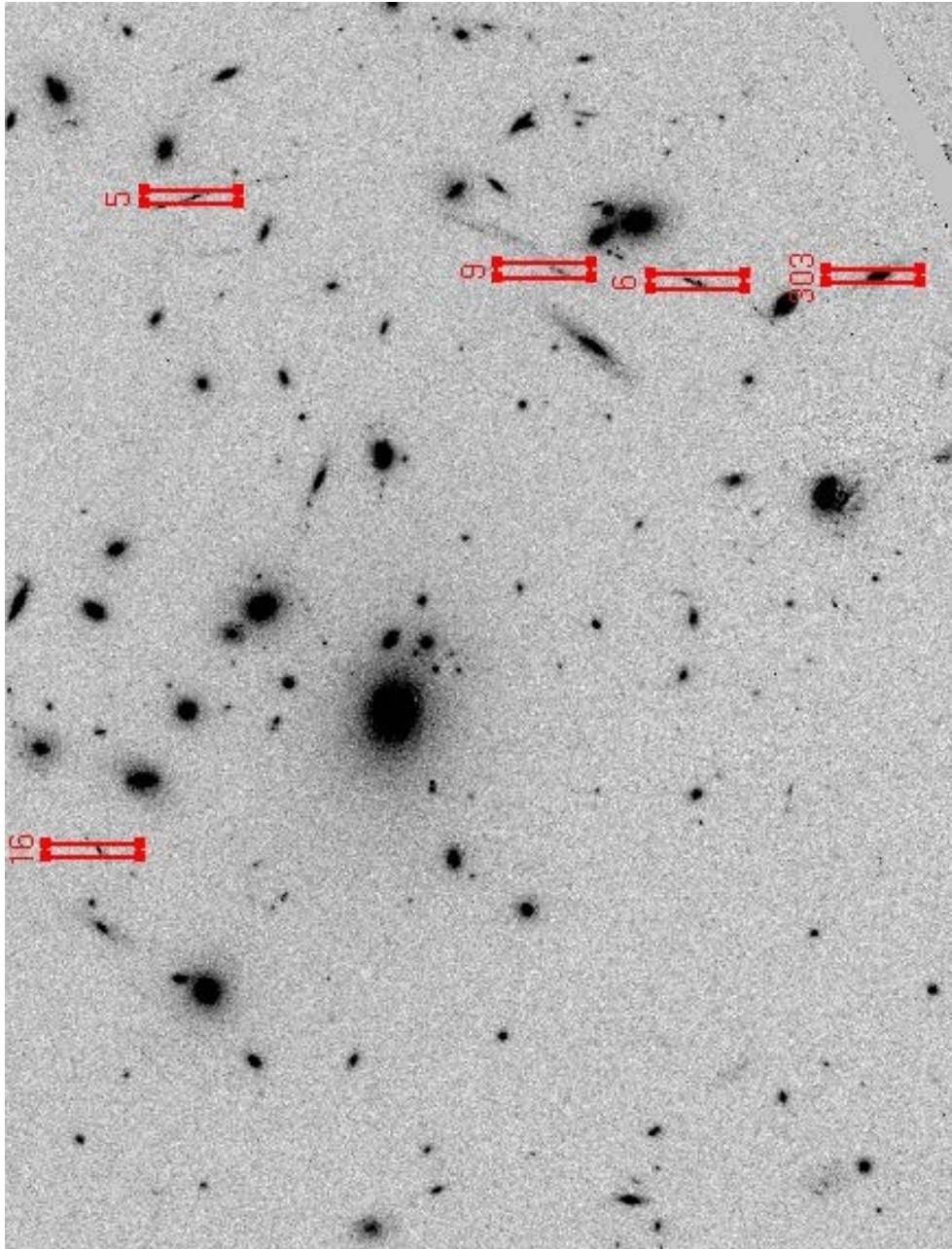


Figure 6.9: The first of two images of the core region of RXCJ2308. The most target-rich cluster in this sample, the core region had too many potential arcs to examine in one mask therefore two separate masks were made for the same cluster. In this image, slits 6 and 9, located in the West of the image sample a region of highly elongated arcs located between the BCG and what appears to be significant cluster substructure to the North-West.

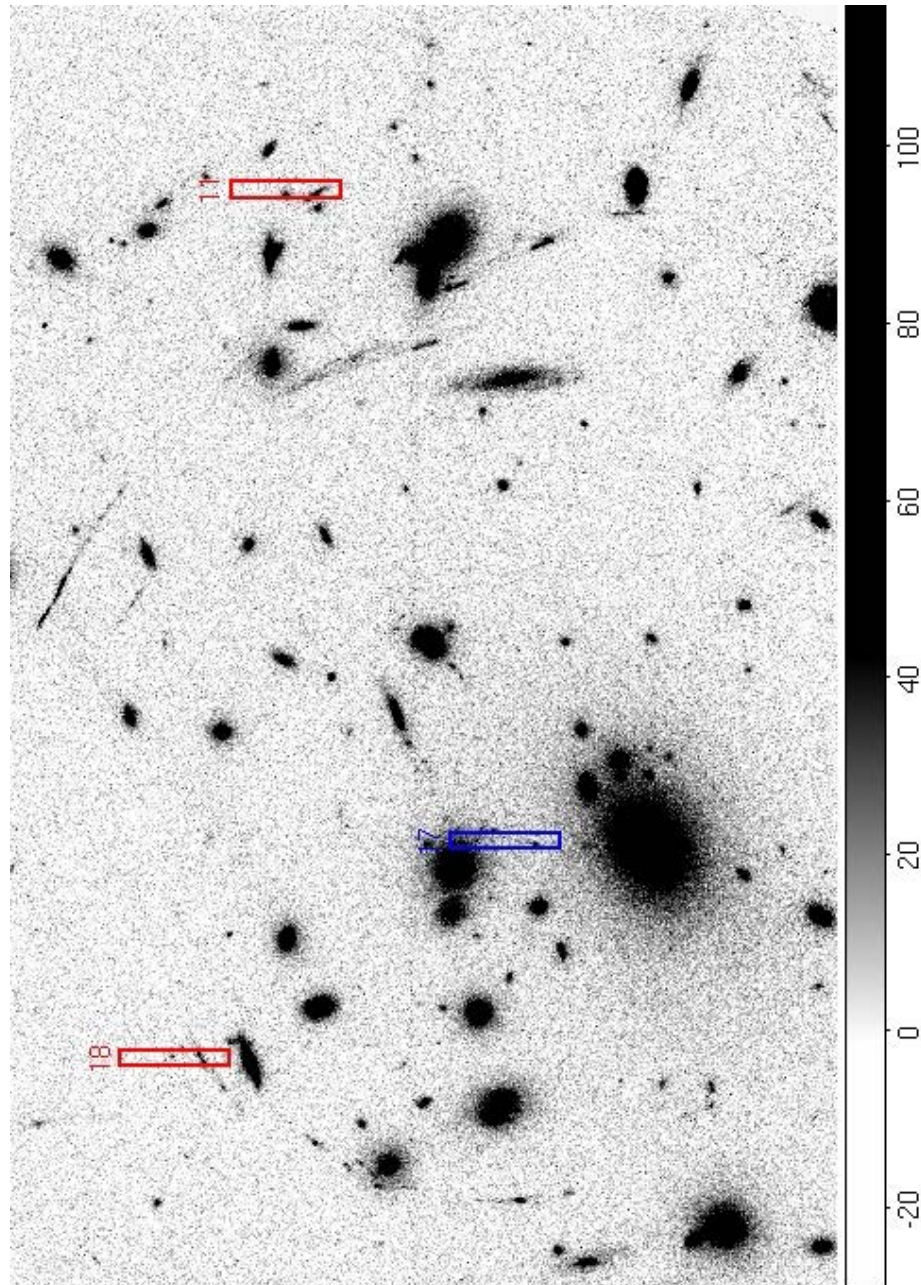


Figure 6.10: The second image of RXCJ2308. Features of note in this frame include sampling of the arc structure in the North-East of the image as well as the targeting of a potential radially aligned arc to the North of the BCG (Slit 17, in blue).

Bibliography

- [1] Matthias Bartelmann and Peter Schneider. Weak gravitational lensing. *Physics Reports*, pages 291–472, 2001.
- [2] Tereasa G. Brainerd, Roger D. Blandford, and Ian Smail. Weak gravitational lensing by galaxies. *The Astrophysical Journal*, pages 623–637, 1996.
- [3] J. S. Bullock, A. V. Kravtsov, and D. H. Weinberg. Reionization and the Abundance of Galactic Satellites. *The Astrophysical Journal*, 539:517–521, 2000.
- [4] D. Clowe and P. Schneider. Wide field weak lensing observations of A1835 and A2204. *Astronomy and Astrophysics*, 395:385–397, 2002.
- [5] F. W. Dyson, A. S. Eddington, and C. Davidson. A Determination of the Deflection of Light by the Sun’s Gravitational Field, from Observations Made at the Total Eclipse of May 29, 1919. *Royal Society of London Philosophical Transactions Series A*, 220:291–333, 1920.
- [6] T. Ebbels. Galaxy evolution from gravitational lensing studies with the hubble space telescope. *PhD Thesis, University of Cambridge*, 1998.
- [7] S. Ghigna, B. Moore, F. Governato, G. Lake, T. Quinn, and J. Stadel. The dark matter substructure of clusters and galaxies. *Observational Cosmology: The Development of Galaxy Systems*, 176:140–+, 1999.
- [8] Jean-Paul Kneib, Richard S. Ellis, Ian Smail, W. J. Couch, and R. M. Sharples. Hubble space telescope observations of the lensing cluster abell 2218. *The Astrophysical Journal*, pages 643–656, 1996.
- [9] E. Komatsu, K. M. Smith, J. Dunkley, C. L. Bennett, B. Gold, G. Hinshaw, N. Jarosik, D. Larson, M. R. Nolte, L. Page, D. N. Spergel, M. Halpern, R. S. Hill, A. Kogut, M. Limon, S. S. Meyer, N. Odegard, G. S. Tucker, J. L. Weiland, E. Wollack, and E. L. Wright. Seven-year Wilkinson Microwave Anisotropy Probe (WMAP) Observations: Cosmological Interpretation. *The Astrophysical Journal*, 192:18–+, February 2011.
- [10] J. Kristian and R. K. Sachs. Observations in cosmology. *The Astrophysical Journal*, page 379, 1966.
- [11] M. Limousin, J. P. Kneib, S. Bardeau, P. Natarajan, O. Czoske, I. Smail, H. Ebeling, and G. P. Smith. Truncation of galaxy dark matter halos in high density environments. *Astronomy and Astrophysics*, 461:881–891, 2007.

- [12] M. Limousin, J. Richard, E. Jullo, J.-P. Kneib, B. Fort, G. Soucaill, Á. Elíasdóttir, P. Natarajan, R. S. Ellis, I. Smail, O. Czoske, G. P. Smith, P. Hudelot, S. Bardeau, H. Ebeling, E. Egami, and K. K. Knudsen. Combining Strong and Weak Gravitational Lensing in Abell 1689. *The Astrophysical Journal*, 668:643–666, October 2007.
- [13] Ramesh Narayan and Matthias Bartelmann. Lectures on gravitational lensing. *arXiv:astro-ph/9606001v2*, 2007.
- [14] P. Natarajan, J.-P. Kneib, I. Smail, T. Treu, R. Ellis, S. Moran, M. Limousin, and O. Czoske. The Survival of Dark Matter Halos in the Cluster Cl 0024+16. *The Astrophysical Journal*, 693:970–983, March 2009.
- [15] Priyamvada Natarajan, Gabriella De Lucia, and Volker Springel. Substructure in lensing clusters and simulations. *Monthly notices of the Royal Astronomical Society*, pages 180–192, 2007.
- [16] Priyamvada Natarajan and Jean-Paul Kneib. Lensing by galaxy haloes in clusters of galaxies. *Monthly notices of the Royal Astronomical Society*, pages 833–847, 1997.
- [17] Priyamvada Natarajan, Jean-Paul Kneib, and Ian Smail. Evidence for tidal stripping of dark matter halos in massive cluster lenses. *The Astrophysical Journal*, pages L11–L15, 2002.
- [18] Priyamvada Natarajan, Jean-Paul Kneib, Ian Smail, and Richard Ellis. Quantifying substructure using galaxy-galaxy lensing in distant clusters. *eprint arXiv:astro-ph/0411426*, 2004.
- [19] Priyamvada Natarajan, Jean-Paul Kneib, Ian Smail, and Richard S. Ellis. The mass/light ratio of early type galaxies: Constraints from gravitational lensing in the rich cluster. *arXiv:astro-ph/9706129v2*, 1998.
- [20] Priyamvada Natarajan, Abraham Loeb, Jean-Paul Kneib, and Ian Smail. Constraints on the collisional nature of the dark matter from gravitational lensing in the cluster a2218. *The Astrophysical Journal*, pages L17–L20, 2002.
- [21] Priyamvada Natarajan and Volker Springel. Abundance of substructure in clusters of galaxies. *The Astrophysical Journal*, pages L13–L16, 2004.
- [22] J. F. Navarro, C. S. Frenk, and S. D. M. White. The Structure of Cold Dark Matter Halos. *The Astrophysical Journal*, 462, May 1996.
- [23] N. Okabe, M. Takada, K. Umetsu, T. Futamase, and G. P. Smith. LoCuSS: Subaru Weak Lensing Study of 30 Galaxy Clusters. *Publications of the Astronomical Society of Japan*, 62:811–, June 2010.
- [24] P Schneider. Introduction to gravitational lensing and cosmology. *astro-ph*, arXiv:astro-ph/0509252v1, 2005.
- [25] Graham P. Smith, Jean-Paul Kneib, Ian Smail, Pasquale Mazzotta, Harald Ebeling, and Oliver Czoske. A hubble space telescope lensing survey of x-ray luminous galaxy clusters - iv. mass, structure and thermodynamics of cluster cores. *Monthly notices of the Royal Astronomical Society*, pages 417–446, 2005.

- [26] G. Soucail, B. Fort, Y. Mellier, and J. P. Picat. A blue ring-like structure, in the center of the A 370 cluster of galaxies. *Astronomy and Astrophysics*, 172:L14–L16, January 1987.
- [27] G. Soucail, Y. Mellier, B. Fort, G. Mathez, and M. Cailloux. The giant arc in A 370 - Spectroscopic evidence for gravitational lensing from a source at $Z = 0.724$. *Astronomy and Astrophysics*, 191:L19–L21, February 1988.
- [28] J. E. Taylor and A. Babul. The evolution of substructure in galaxy, group and cluster haloes - III. Comparison with simulations. *Monthly Notices of the Royal Astronomical Society*, 364:535–551, 2005.
- [29] J. A. Tyson. Deep CCD survey - Galaxy luminosity and color evolution. *The Astrophysical Journal*, 96:1–23, July 1988.
- [30] K. Umetsu and N. Okabe. Subaru Weak Lensing Study of Merging Clusters of Galaxies. *Astronomical Society of the Pacific Conference Series*, 399:111–+, 2008.
- [31] D. Walsh, R. F. Carswell, and R. J. Weymann. 0957 + 561 A, B - Twin quasistellar objects or gravitational lens. *Nature*, 279:381–384, May 1979.
- [32] G. Wilson, N. Kaiser, G. A. Luppino, and L. L. Cowie. Galaxy Halo Masses from Galaxy-Galaxy Lensing. *The Astrophysical Journal*, 555:572–584, 2001.
- [33] F. Zwicky. Nebulae as gravitational lenses. *Phys. Rev.*, 51(4):290, Feb 1937.